FRONTIERS OF PHYSICS

REVIEW ARTICLE
Volume 21 / Issue 5 / 055303 / 2026

Magnetization processes in metallic Shastry–Sutherland systems: A comprehensive review

Pavol Farkašovský†, Lubomíra Regeciová

Institute of Experimental Physics, Slovak Academy of Sciences, Watsonova 47, 040 01 Košice, Slovakia
Corresponding author. E-mail: †farky@saske.sk
Received January 13, 2026; accepted April 20, 2026

© Higher Education Press 2026

ABSTRACT

Rare-earth tetraborides RB_4 are unique frustrated magnets in which strongly anisotropic localized $4f$ moments coexist with itinerant $5d$ electrons on the geometrically frustrated Shastry–Sutherland lattice. Their magnetization curves display remarkably rich sequences of fractional plateaus, ranging from the robust $1/2$ state in ErB_4 and TmB_4 to intricate cascades in HoB_4 and TbB_4, whose microscopic origins cannot be captured by localized-spin models alone. This review provides a comprehensive and unified theoretical picture of the mechanisms that stabilize these commensurate magnetic textures. We begin with long-range oscillatory RKKY interactions that naturally emerge from the metallic character of the RB_4 compounds and show how accurate numerical treatment reveals a dense hierarchy of competing plateau phases. We then move to explicit spin-electron models, where electron itinerancy, Coulomb repulsion, transverse exchange terms, and realistic mixed-spin configurations jointly reconstruct the plateau stability diagram and reproduce the dominant experimental features. Further extensions, such as the coupled double-Ising (CDI) mapping and charge-stripe potentials, reveal how subtle electronic textures selectively suppress or enhance magnetization plateaus, enabling microscopic control over the competition between the 1/3 and 1/2 plateaus and linking magnetization processes to the magnetocaloric response. The theoretical frameworks reviewed here establish that the interplay of geometrical frustration, itinerant electrons, electronic correlations, and exchange anisotropy is essential for understanding the magnetic and thermodynamic behavior of metallic Shastry–Sutherland materials. The resulting picture not only explains the material-dependent plateau sequences observed in rare-earth tetraborides but also provides a versatile platform for designing new frustrated magnets with tunable fractional states and enhanced magnetocaloric performance.

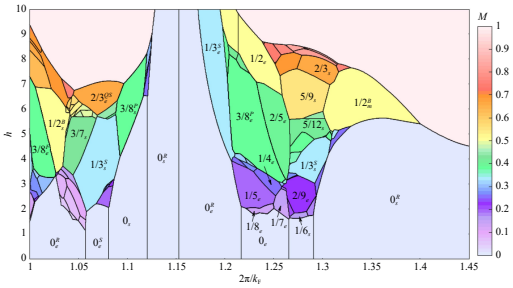

Keywords Shastry–Sutherland magnets, magnetization processes, rare-earth tetraborides, frustrated magnetism, spin–electron models, RKKY interaction

Contents

1 Introduction

Models defined on the Shastry–Sutherland lattice (SSL) constitute one of the most prominent realizations of geometrically frustrated spin systems in condensed-matter physics. It can be visualized as a square lattice with antiferromagnetic couplings between nearest-neighbour spins and additional antiferromagnetic couplings between next-nearest-neighbour spins in every second square. These diagonal interactions introduce strong geometrical frustration and lead to an extensive ground-state degeneracy that gives rise to a variety of exotic magnetic phenomena. Although originally conceived as a purely theoretical construction by Shastry and Sutherland [1], it gradually evolved into a prototypical platform for studying frustrated magnetism.

A major breakthrough occurred when a real material was discovered to host precisely the same lattice geometry. The first and most famous experimental realization of the SSL is the insulating quantum magnet $SrCu_2(BO_3)_2$ [2–9]. In this compound, the Cu^{2+} ions form orthogonal dimer pairs arranged exactly as in the Shastry–Sutherland model [Fig. 1(a)], with a dominant intradimer coupling J_2 and a weaker interdimer coupling J_1 [Fig. 1(b)]. Because $SrCu_2(BO_3)_2$ is an electrical insulator, its low-energy physics is governed entirely by localized spins, making it an ideal platform for testing theoretical approaches based on the Heisenberg Hamiltonian [10–14]. A broad spectrum of theoretical techniques ranging from the Monte Carlo methods, linked-cluster expansions, and continuous unitary transformations [15–17] to modern tensor-network methods [18–21], has been applied to this system. These studies successfully explain a number of hallmark features: the exact dimerized ground state [1], strongly localized triplet excitations [22], and a cascade of magnetization plateaus at $m/m_s = 1/8$, $2/15$, $1/6$, $1/4$, $1/3$, and $1/2$, observed experimentally in high magnetic fields up to 120 T [23–25]. The exceptional agreement between theory and experiment firmly established $SrCu_2(BO_3)_2$ as the prototypical realization of the Shastry–Sutherland model and demonstrated that the SSL framework captures the essential microscopic physics behind the plateau formation in quantum magnets. This success naturally motivated the search for further materials with the same lattice geometry. In this context, two distinct directions have emerged. On one hand, several insulating SSL compounds have been identified, in which the magnetization process is governed predominantly by localized spin interactions [26–28]. A second, and in many respects even more remarkable, family of SSL-based compounds is found among the metallic rare-earth tetraborides RB_4 (R = La–Lu) [29–35]. Although their bonding arrangement is topologically equivalent to that in $SrCu_2(BO_3)_2$, the tetraborides differ in several crucial aspects. Structurally, the SSL is slightly distorted: the diagonal angle is shifted, which leads to nearest- and next-nearest-neighbour exchange integrals that are nearly equal in magnitude, $J_1 \approx J_2$ as shown in Fig. 1(c). This near-degeneracy enhances the geometrical frustration far beyond that found in $SrCu_2(BO_3)_2$. Even more importantly, the tetraborides are metallic: $4f$ moments of the rare-earth ions coexist with itinerant $5d$ electrons that mediate additional interactions and couple strongly to the magnetic order [36]. The rare-earth ions occupy the positions of the SSL in the ab plane of the tetragonal $P4/mbm$ crystal structure, again forming the characteristic

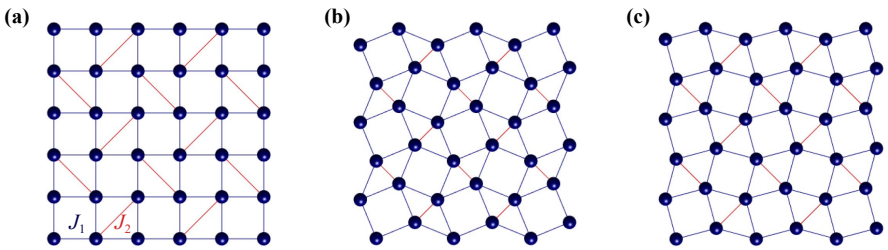

Fig. 1 The original Shastry–Sutherland lattice with the first J_1 and second J_2 nearest-neighbour couplings **(a)**, and the topologically identical Archimedian lattice [37] realized in the $SrCu_2(BO_3)_2$ **(b)** and rare-earth tetraborides RB_4 **(c)**.

network of squares and orthogonal diagonals. In this setting, the combination of localized and itinerant degrees of freedom on a strongly frustrated SSL creates an unusually rich magnetic behaviour.

The experimental discovery of series of fractional magnetization plateaus at low temperatures in the rare-earth tetraborides has attracted enormous attention during the last two decades [38–41]. Magnetization measurements have revealed a fascinating sequence of plateaus, the positions and widths of which depend strongly on the particular rare-earth element. For instance, in HoB_4 the plateaus occur at $m/m_s = 1/3, 4/9,$ and $3/5$ [41–43]; in TbB_4 at $m/m_s = 2/9, 1/3, 4/9, 1/2,$ and $7/9$ [44]; in ErB_4 a single broad plateau is observed at $m/m_s = 1/2$ [41, 45]; and in TmB_4 the sequence consists of a dominant $1/2$ plateau accompanied by a very narrow metastable ones [29, 36, 50, 51]. The existence of such fractional plateaus is considered the most prominent manifestation of geometrical frustration in these metallic systems. It reflects the stabilization of magnetically ordered states with a large unit cell and provides an important experimental benchmark for theoretical modelling.

In addition to the magnetization measurements, many other experimental techniques, such as specific-heat [52–54], magnetotransport [45, 46, 55], and magnetocaloric measurements [56–58], have been employed to explore the thermodynamic and dynamic properties of RB_4 compounds. These studies confirmed the strongly anisotropic magnetic behaviour and revealed a complex interplay between localized $4f$ moments of the rare-earth ions and itinerant $5d$ electrons that are responsible for the metallic conductivity. From this viewpoint, the rare-earth tetraborides represent a unique class of materials in which the localized and itinerant subsystems coexist and interact on the geometrically frustrated SSL. This dual character requires theoretical models capable of describing both local-moment interactions and itinerant-electron effects on an equal footing.

1.1 Historical development of theoretical approaches

The first theoretical efforts to explain the fractional magnetization plateaus in RB_4 naturally started from pure spin models. Because of the strong single-ion anisotropy imposed by the crystal field, the localized moments R^{3+} can be, in the first approximation, treated as Ising spins. The simplest model that captures the geometry of the lattice is therefore the Ising model on the SSL, characterized by the couplings J_1 and J_2. Analytical and numerical studies of this model have shown that it stabilizes only a single fractional plateau at $m/m_s = 1/3$ [59–61]. This $1/3$ plateau corresponds to a configuration in which one third of the spins are aligned antiparallel to the external magnetic field, while the remaining two thirds point parallel to it, forming a stripe-like pattern. The success of this model lies in its ability to reproduce the basic mechanism of plateau formation in a frustrated geometry and to provide a clear physical picture based solely on localized spins with strong Ising anisotropy.

However, the limitations of this minimal model became apparent when compared with experimental data. In particular, the absence of the $1/2$ plateau, the most pronounced feature in ErB_4 and TmB_4, and the inability to reproduce the more complex plateau sequences observed in other compounds indicate that the nearest- and next-nearest-neighbour Ising model is not sufficient to capture the magnetic behaviour of real RB_4. To improve the agreement with experiments, several generalizations of the classical Ising model were proposed. These extensions included longer-range interactions and additional multispin terms [62–68]. It was demonstrated that such generalized models can, for some combinations of parameters, stabilize additional plateaus, including the experimentally observed $1/2$ plateau. Nevertheless, these modifications significantly increase the number of adjustable parameters, and it is often difficult to assign them a clear microscopic origin. In practice, the stability of individual plateaus in such models depends sensitively on the chosen values of the exchange constants, which limits their predictive power.

A further improvement was achieved by incorporating quantum fluctuations through Heisenberg or XXZ-type models on the SSL [69, 70]. In the spin-$1/2$ Heisenberg model, for example, the competition between J_1 and J_2 gives rise to a rich phase diagram including a dimerized singlet ground state, Néel-like order, and intermediate phases with complex spin textures. Quantum Monte Carlo and exact-diagonalization studies revealed that a moderate transverse component of the exchange can partially suppress the Ising-like $1/3$ plateau and lead to the emergence of additional plateau at $m/m_s = 1/2$. However, the parameter region in which these features appear is usually narrow, and the required anisotropy is often unrealistically large for real tetraborides. Therefore, although the inclusion of quantum effects enriches the theoretical phase diagram, it still does not provide a fully satisfactory quantitative description of the experimental magnetization curves.

The main conceptual problem of all purely spin models lies in their neglect of the metallic character of the rare-earth tetraborides. In these systems, the magnetic R^{3+} ions interact not only via direct exchange but also indirectly through conduction electrons occupying the $5d$ bands. The evidence for this comes from measurements of electrical resistivity and magnetotransport, which reveal metallic conduction and strong coupling between magnetic order and the electronic subsystem [45, 46]. Consequently, the effective magnetic interactions [36] are expected to have a long-range, oscillating character of the Ruderman–Kittel–Kasuya–Yosida (RKKY) type [47–49]. Such interactions naturally extend beyond the

nearest neighbours and can therefore provide a microscopic justification for the longer-range couplings that are otherwise added empirically to classical Ising models.

Another limitation of spin-only descriptions is their inability to capture the mutual influence between itinerant electrons and localized moments. In real materials, the conduction electrons can mediate effective interactions between localized spins, modify their exchange integrals, and, conversely, the magnetic ordering can affect the electronic density of states and transport properties. This mutual feedback is completely absent in models that consider spins as isolated from the itinerant background. It is thus reasonable to expect that a realistic theoretical description of RB_4 should explicitly include both subsystems and their coupling.

1.2 Motivation and scope of this review

The shortcomings of the pure spin approach have stimulated the development of several complementary theoretical frameworks that take the itinerant electrons into account either indirectly, through effective long-range RKKY interactions, or directly, by coupling localized spins with itinerant electrons in combined spin-electron Hamiltonians. The first line of research, based on the generalized Ising model with RKKY interactions, successfully reproduces the appearance of new magnetization plateaus and provides a microscopic mechanism rooted in the oscillatory exchange mediated by conduction electrons [71–75]. The second line, represented by spin-electron and extended Hubbard models on the SSL [76–83], offers an explicit treatment of both subsystems and reveals how their mutual coupling can lead to complex magnetic and thermodynamic behaviour.

In the present review, we aim to provide a comprehensive overview of these developments with a particular emphasis on the role of itinerant electrons in stabilizing various magnetic states on the SSL. Starting from the earliest RKKY-based studies, we will trace the gradual evolution towards more elaborate spin–electron and Hubbard-type models and discuss how these frameworks overcome the limitations of purely localized spin descriptions. While the detailed results of these approaches will be presented in the subsequent sections, the main goal of this introductory part is to outline the experimental motivation, summarize the key findings and shortcomings of the classical spin models, and justify the necessity of including the electronic degrees of freedom explicitly in the theoretical treatment of magnetization processes in the Shastry–Sutherland rare-earth tetraborides.

2 RKKY interaction and indirect electron coupling effects

In view of the metallic nature of rare-earth tetraborides and the evident limitations of purely localized-spin descriptions, the next logical step in the theoretical treatment of Shastry–Sutherland magnets is to consider the effect of conduction electrons on the effective magnetic interactions between localized moments. Since the direct inclusion of itinerant electrons in a microscopic model considerably increases its complexity, an attractive intermediate approach consists in taking the itinerant degrees of freedom into account indirectly, through the oscillatory exchange interaction mediated by the conduction electrons – the Ruderman–Kittel–Kasuya–Yosida (RKKY) mechanism. The RKKY interaction naturally introduces both ferromagnetic and antiferromagnetic couplings that alternate in sign and range depending on the Fermi momentum $k_{\rm F}$, thereby providing a microscopic origin for the long-range competing interactions that were earlier introduced empirically into the classical Ising models.

2.1 Early RKKY approach and the origin of magnetization plateaus

The first systematic attempt to describe the magnetization process of metallic rare-earth tetraborides using an RKKY-type interaction was carried out by Feng *et al.* [71]. Their work demonstrated that the long-range, oscillatory exchange mediated by conduction electrons can by itself generate a sequence of fractional magnetization plateaus on the SSL, without invoking higher-order or multi-spin interactions. In this approach the localized Ising spins $S_i = \pm 1$ interact via the three-dimensional RKKY exchange derived for an isotropic free-electron gas. The Hamiltonian is

$$H = \sum_{ij} J(r_{ij})\, S_i S_j - h \sum_i S_i, \tag{1}$$

where the indirect exchange coupling takes the analytic 3D RKKY form

$$J(r_{ij}) = -J_0 a^3 \left[\frac{\cos(2k_{\rm F} r_{ij})}{r_{ij}^3} - \frac{\sin(2k_{\rm F} r_{ij})}{2k_{\rm F} r_{ij}^4} \right], \tag{2}$$

with $J_0 > 0$ setting the overall scale, a the lattice constant, and $k_{\rm F}$ the Fermi wave vector. Because $J(r_{ij})$ oscillates and changes sign with distance, the interaction naturally generates competing ferro- and antiferromagnetic bonds across multiple coordination shells.

Feng *et al.* [71] considered a 24×24 SSL cluster with periodic boundaries and evaluated all RKKY couplings up to a cut-off of $r_{\rm max} = 6a$. For the reference Fermi wave vector $k_{\rm F} = 2\pi/1.243$, corresponding to the estimated conduction-electron density of TmB_4, the magnetization curve exhibits four distinct steps at low temperature: a q-Néel antiferromagnetic state $L(0)$, a narrow 1/4 plateau corresponding to $U(1/4)$ state, a wide and robust 1/2 plateau associated with a ferrimagnetic $Z(1/2)$ configu-

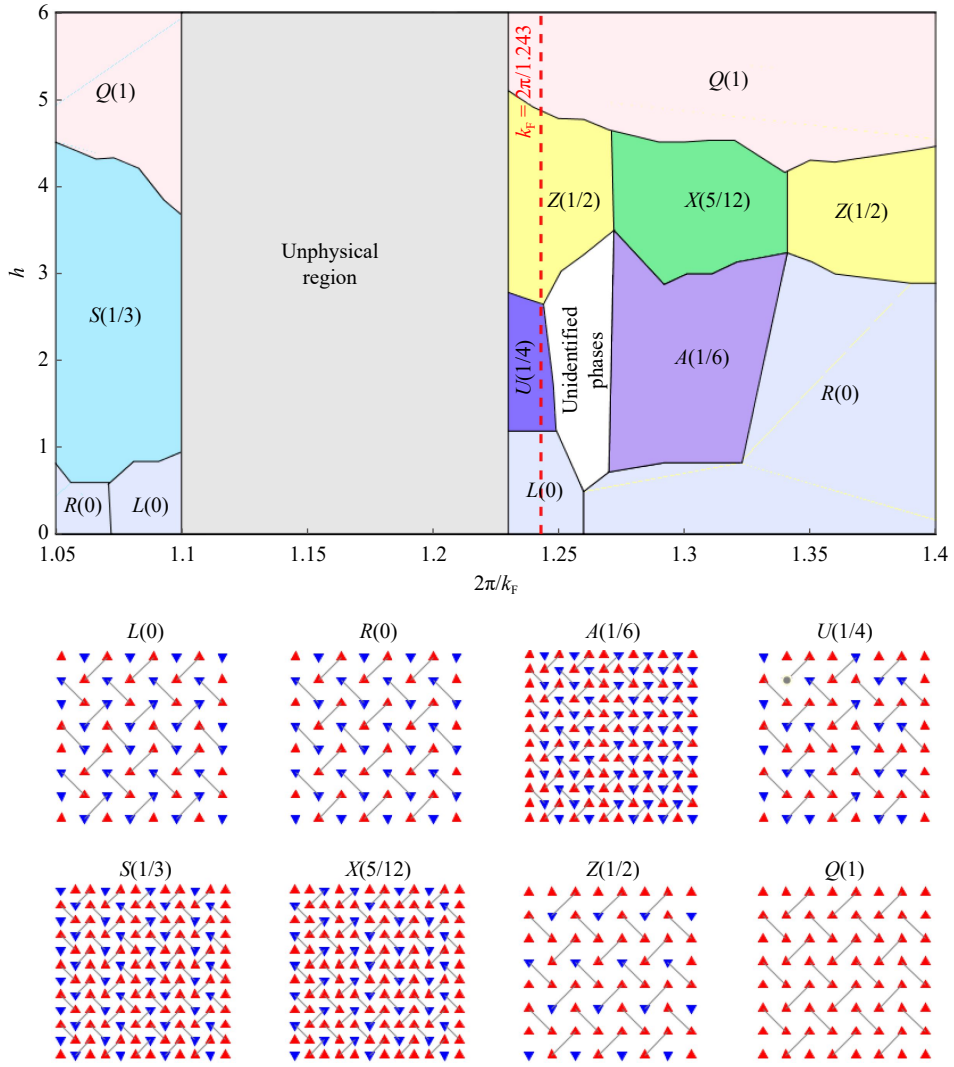

Fig. 2 Magnetic phase diagram of the Ising model on the Shastry–Sutherland lattice with the 3D RKKY interaction from Ref. [71]. The reference case $k_F = 2\pi/1.243$ contains a narrow 1/4 plateau and a robust 1/2 plateau. Representative real-space spin configurations corresponding to the dominant ordered phases are shown below the diagram. Upward (▲) and downward (▼) triangular markers denote spins aligned parallel and antiparallel to the external magnetic field, respectively; the same notation is used throughout the manuscript.

ration, and a fully saturated ferromagnetic $Q(1)$ phase (see Fig. 2). The 1/4 plateau vanishes already at $T \approx 0.1$, whereas the 1/2 plateau remains stable up to $T \approx 0.4$. This strong thermal stability of the 1/2 plateau is a direct consequence of the RKKY-induced balance between further-neighbour couplings, which favours the $Z(1/2)$ structure over all competing arrangements.

A key result is the strong sensitivity of the plateau sequence to the value of k_F. This sensitivity originates from the fact that the sign and magnitude of the effective next-neighbour interactions (J_3, J_4, J_5,...) change rapidly with k_F. For k_F close to $2\pi/1.243$ the $Z(1/2)$ state is energetically preferred, stabilizing the 1/2 plateau. Decreasing k_F towards $2\pi/1.100$ reverses the sign of J_3 and weakens the ferromagnetic J_5 term, which favours the UUD configuration and generates a clear 1/3 plateau. In contrast, for smaller values such as $k_F = 2\pi/1.300$, the model supports new commensurate structures producing additional plateaus at $m/m_s = 1/6$ and 5/12. These trends are in direct correspondence with the oscillatory character of the RKKY exchange and illustrate how the conduction electrons tune the competition between distinct magnetic superstructures.

Altogether, the work of Feng *et al.* [71] demonstrated that the RKKY interaction is not only capable of stabilizing the experimentally important 1/2 plateau, but can also generate a hierarchy of additional fractional steps whose stability is controlled by the electronic density. In this picture, the Fermi wave vector plays the role of a microscopic tuning parameter that selects between competing commensurate magnetic textures, providing a natural explanation for the strong sample-to-sample variation of

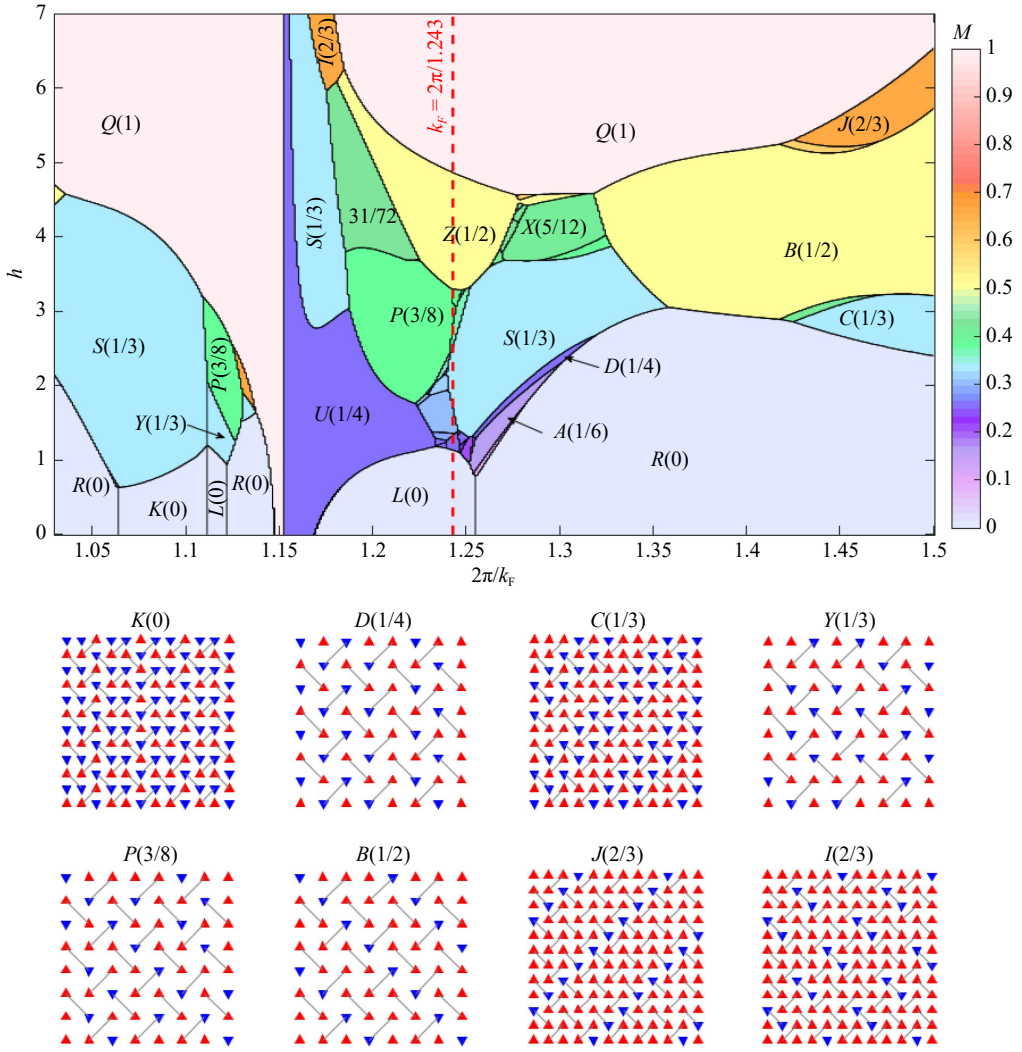

Fig. 3 Magnetic phase diagram of the 2D Ising model on the SSL with the 3D RKKY interaction calculated for the $L = 24 \times 24$ cluster from Ref. [72]. The additional representative spin configurations corresponding to the main ordered phases are shown below the diagram.

plateau sequences observed in metallic rare-earth tetraborides.

2.2 Numerical refinement and phase-diagram complexity

In order to verify the conclusions of Feng *et al.* [71] and to test the robustness of the 1/2 plateau predicted by their model, Regeciová and Farkašovský revisited the problem in Ref. [72], introducing substantial improvements in both numerical precision and physical realism. Their study re-examined the same RKKY-based Ising model on the SSL [see Eq. (1) and Eq. (2) in Section 2.1 for the Hamiltonian and interaction definition], but used a careful finite-size scaling, refined statistical averaging, and an updated computational scheme combining the Metropolis algorithm [84] with parallel tempering [85]. The main goal was to determine whether the sequence of magnetization plateaus and corresponding phase boundaries found by Feng *et al.* [71] were intrinsic to the model or artefacts of finite-size limitations and insufficient sampling.

These improvements dramatically changed the resulting magnetization process. Instead of the simple four-phase structure reported earlier, the refined simulations revealed a much richer hierarchy of fractional plateaus. Besides the $m/m_s = 1/2$ state, several additional commensurate phases were found, including plateaus at $m/m_s = 1/3, 3/8$, as well as multiple narrower intermediate steps. All of these plateaus persist across system sizes and appear systematically once metastable states are fully eliminated. The presence of these additional fractions demonstrates that the RKKY-Ising model has an intrinsically complex energy landscape whose structure cannot be resolved without careful annealing and large clusters.

The corresponding ground-state phase diagram obtained in the (k_F, h) plane is shown in Fig. 3. In

contrast to earlier results, the improved diagram contains multiple ferrimagnetic and modulated phases separated by distinct first-order boundaries. The fractional plateaus arise from subtle competition between several coordination shells of the oscillatory RKKY exchange, and their stability depends sensitively on the value of the Fermi momentum. Small changes of k_F around $k_F = 2\pi/1.243$, simulating electron or hole doping, reorganize the plateau sequence and shift the critical fields.

In summary, the refined numerical analysis showed that the appearance of multiple fractional plateaus is an intrinsic feature of the RKKY interaction on the SSL. The mixed 3D–2D formulation, which reflects the real electronic dimensionality of rare-earth tetraborides, naturally reproduces a broad set of commensurate spin textures and provides a microscopic origin for the material-dependent magnetization behaviour observed experimentally.

2.3 Two-dimensional RKKY interaction and the role of electronic dimensionality

While the mixed 3D–2D formulation provided a major improvement over the earlier model of Feng *et al.* [71], the use of a three-dimensional Fermi surface to describe conduction electrons remained a simplification that could not fully capture the layered electronic structure of the rare-earth tetraborides. Angle-dependent magnetotransport experiments on TmB_4 revealed a strongly anisotropic Fermi surface [55], implying that the effective exchange between localized moments should be derived for a two-dimensional electron gas. This observation motivated a further refinement of the theory, presented in Ref. [73], where the RKKY interaction was reformulated for two-dimensional conduction electrons.

In this version of the model, the localized spins on the SSL were again treated as classical Ising variables, but the coupling between them was obtained from the 2D analogue of the RKKY interaction [86]:

$$J(r_{ij}) = \frac{k_F^2}{2\pi}\left[B_0^{(1)}(k_F r_{ij})\, B_0^{(2)}(k_F r_{ij}) + B_1^{(1)}(k_F r_{ij})\, B_1^{(2)}(k_F r_{ij})\right], \quad (3)$$

where $B_n^{(1)}(x)$ and $B_n^{(2)}(x)$ are the Bessel functions of the first and second kind, respectively. This expression retains the characteristic oscillatory behaviour of the indirect exchange but exhibits a slower spatial decay than its three-dimensional counterpart, reflecting the longer-ranged character of the interaction in a two-dimensional electron gas. The modified form of $J(r_{ij})$ is thus more realistic for the metallic SSL layers in the tetraborides, where conduction electrons are largely confined to the *ab* plane but can still mediate effective couplings between distant sites.

Comprehensive Monte Carlo simulations were again performed using the combination of Metropolis updates and parallel tempering up to $L = 120 \times 120$ clusters. The resulting phase behaviour was mapped as a function of the Fermi momentum k_F and external magnetic field h, producing the phase diagram shown in Fig. 4. The most notable feature of this diagram is the broad stability region of the $m/m_s = 1/2$ plateau that dominates over a wide range of k_F values in the central part of the phase diagram (near the point $k_F = 2\pi/1.25$), and the total absence of the $m/m_s = 1/3$ plateau, in striking correspondence with the experimental magnetization of ErB_4. For slightly smaller k_F, corresponding to lower carrier concentrations, a cascade of narrow plateaus appears below $m/m_s = 1/2$, reminiscent of the magnetization process observed in TmB_4.

From a physical point of view, the transition from the three-dimensional to the two-dimensional RKKY form has several important consequences. First, the interaction oscillates with a different period and slower amplitude decay, which modifies the hierarchy of effective exchange integrals within the SSL. As a result, the competition among the first few coordination shells becomes less pronounced, and the magnetic frustration is partly relieved. This leads to a simplification of the magnetization curve: the multitude of fractional plateaus present in the 3D–2D model collapses into a single dominant plateau at 1/2, accompanied by a few narrow phases at lower magnetizations.

In this study, the authors systematically explored several values of the Fermi momentum, effectively simulating the influence of electron and hole doping on the two-dimensional RKKY interaction. Changes in k_F modify the oscillation period of the indirect exchange and thus alter the relative stability of fractional plateaus. This provides a clear microscopic interpretation of how carrier doping can tune the magnetization

2.4 Three-dimensional RKKY coupling and the hierarchy of fractional plateaus

To complete the systematic analysis of dimensionality effects, Regeciová and Farkašovský extended their approach to the case where both the magnetic lattice and the electronic subsystem are treated as fully three-dimensional [74]. This "3D–3D" model was designed to explore the impact of interlayer magnetic coupling and to determine whether the inclusion of interplane interactions could reproduce the entire diversity of magnetization plateaus observed experimentally across the rare-earth tetraboride family.

The Hamiltonian and interaction form used here are the same as those introduced in Section 2.1 [see Eqs. (1) and (2)]. In this configuration, the exchange network couples each spin not only to its in-plane neighbours but also to sites in adjacent layers, thereby introducing an additional source of frustration that enriches the

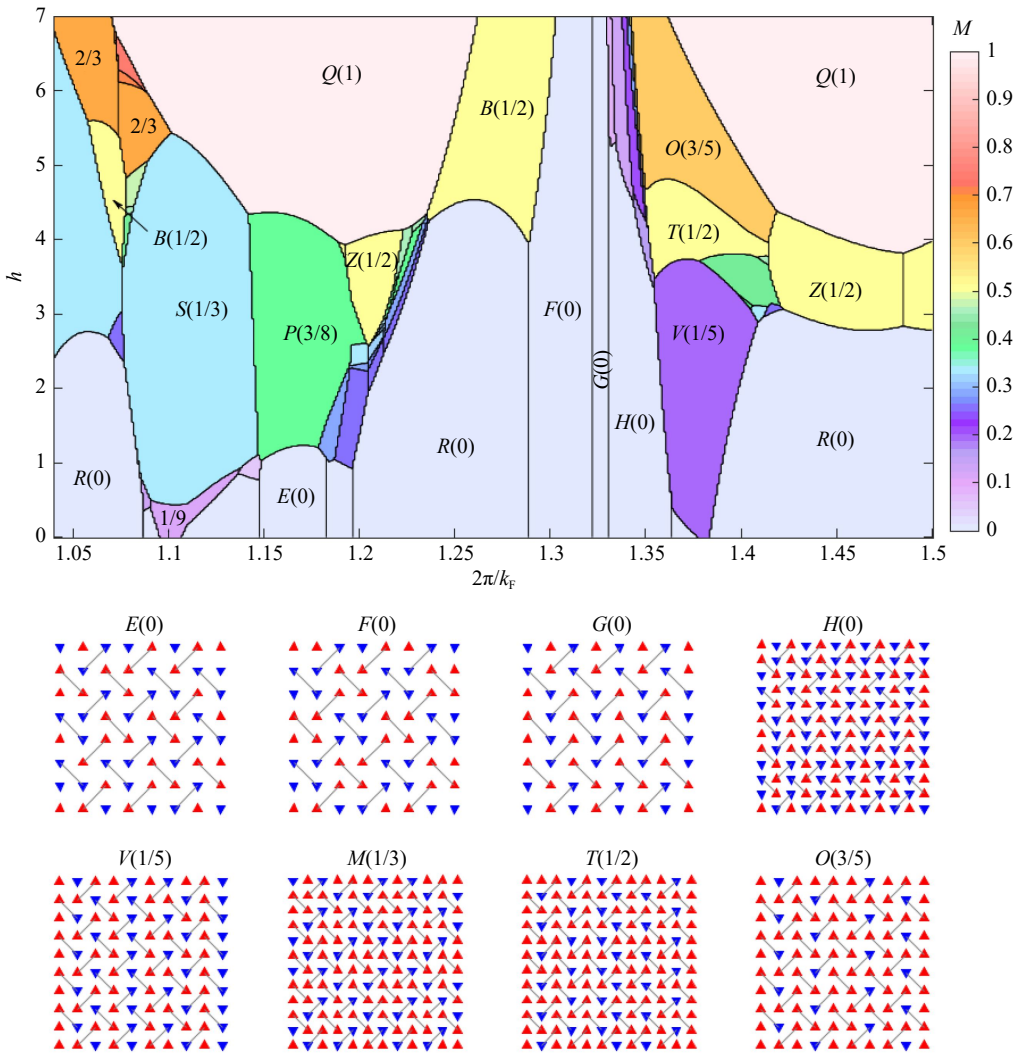

Fig. 4 Magnetic phase diagram of the Ising model on the SSL with the two-dimensional RKKY interaction calculated for the $L = 120 \times 120$ cluster from Ref. [73]. New representative spin configurations corresponding to the main phases are shown below the diagram.

magnetic phase space.

Monte Carlo simulations were performed on cubic clusters ranging from $L = 12 \times 12 \times 12$ up to $L = 20 \times 20 \times 20$, using the standard Metropolis algorithm supplemented by parallel tempering to reduce metastability. For each pair (h, k_F) the system was cooled down to the lowest temperature $T = 0.05$, and the resulting spin configuration was used to evaluate the approximate ground-state energy. To minimize finite-size effects, this procedure was repeated for all cluster sizes, and the physical magnetization m was assigned by selecting the value $m(L)$ corresponding to the lowest-energy configuration among all L. Applying this minimization procedure over the entire (h, k_F) parameter space yields the magnetic phase diagram shown in Fig. 5, which displays an exceptionally rich hierarchy of ferrimagnetic, striped, and modulated phases with numerous fractional magnetization plateaus. Stable plateaus were identified at $m/m_s = 1/8, 1/7, 1/6, 1/5, 2/9, 1/4, 1/3, 3/8, 2/5, 5/12, 3/7, 1/2, 5/9$, and $2/3$, which collectively reproduce almost all fractional magnetization values reported in TmB_4, TbB_4, HoB_4, and ErB_4.

From a physical viewpoint, the inclusion of the third dimension leads to a much stronger competition among exchange paths. Whereas the two-dimensional model stabilizes essentially a single dominant $1/2$ plateau, the three-dimensional one supports a cascade of fractional plateaus reflecting the coexistence of multiple commensurate superstructures. The simulation results clearly indicated that small variations of the Fermi momentum k_F, which can correspond to changes in carrier concentration due to doping, strongly modify the sequence and stability of the plateaus. In particular, for k_F values characteristic of rare-earth tetraborides, the model predicts the presence of the $1/8$ plateau that had been previously observed experimentally but was absent in

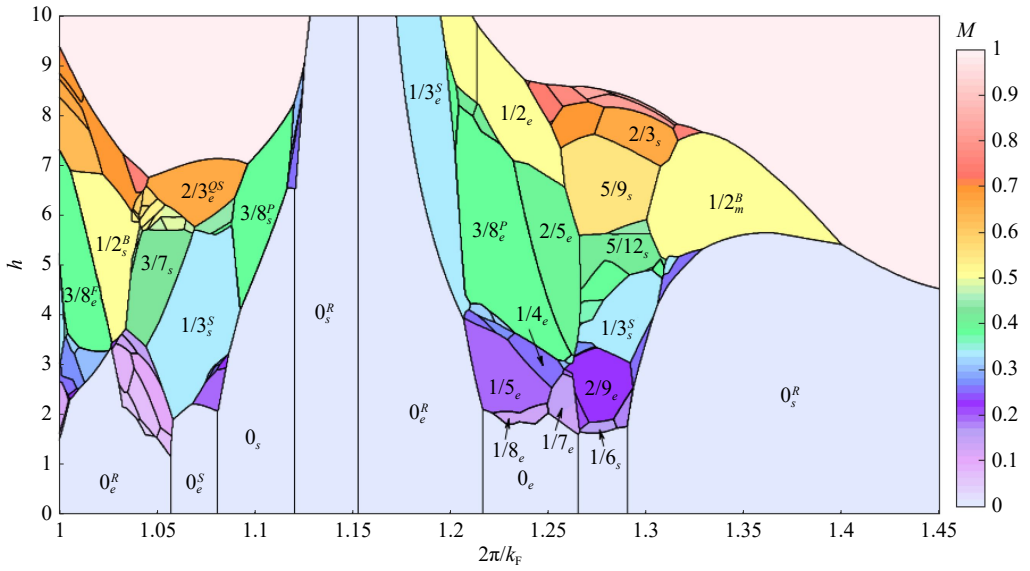

Fig. 5 Magnetic phase diagram of the Ising model on the three-dimensional stack of Shastry–Sutherland layers with the 3D RKKY interaction [74]. The upper index in each phase label denotes the intraplane spin configuration (see Figs. 2–4), i.e., the two-dimensional ordering pattern within a single Shastry–Sutherland layer. The lower index specifies the interplane arrangement along the c-axis: e indicates identical stacking of layers, s (or m) denotes layers that are identical but mutually shifted (or mirrored), and c corresponds to an alternating sequence of layers with different intraplane configurations (and often different magnetizations).

the 2D approximation.

In addition to the reference region corresponding to the undoped compounds, the study systematically examined slightly lower and higher k_F values to simulate hole and electron doping. These variations in the Fermi momentum effectively model changes in carrier concentration and allow one to track how doping reorganizes the competition between exchange shells. The resulting shifts of the plateau boundaries and the emergence or suppression of specific fractional states demonstrate that doping provides a direct microscopic mechanism for tuning the magnetic phase diagram of metallic Shastry–Sutherland systems. The 3D–3D RKKY model therefore represents the most complete indirect-electron description to date, capable of reproducing the experimentally observed complexity of magnetization processes in rare-earth tetraborides.

2.5 Magnetocaloric effect within the 2D–2D RKKY model

In addition to reproducing the fractional magnetization plateaus, the RKKY framework also offers a microscopic explanation of the anomalous magnetocaloric properties observed in the metallic rare-earth tetraborides. The work [75] investigated this effect within the two-dimensional Ising model on the Shastry–Sutherland lattice coupled by the two-dimensional RKKY interaction. This formulation, in which both the magnetic and electronic subsystems are restricted to the plane, was motivated by the strongly anisotropic and quasi-two-dimensional Fermi surface experimentally confirmed in TmB_4.

The same Hamiltonian was adopted as in the preceding RKKY studies, with the coupling $J(r_{ij})$ given by the two-dimensional RKKY expression Eq. (3). Monte Carlo simulations on the 24×24 cluster combined with parallel tempering were employed to evaluate the temperature- and field-dependent entropy change $\Delta S(T,h) = S(T,h) - S(T,0)$ [75]. The calculated results, summarized in Fig. 6, show a pronounced non-monotonic field dependence of ΔS. A positive "heating" peak appears near the metamagnetic transition between fractional plateaus, followed by a negative "cooling" valley at higher fields. This alternating behaviour reproduces the main features of the experimental magnetocaloric response of TmB_4.

In this work, the magnetocaloric quantities were computed for several representative Fermi momenta, which effectively simulate changes in the carrier concentration due to electron or hole doping. Varying k_F modifies the oscillatory character of the RKKY interaction and therefore shifts the position and amplitude of the heating and cooling peaks in ΔS. This analysis revealed that doping can strongly enhance or suppress the magnetocaloric efficiency, and that there exist two distinct intervals of k_F corresponding to maximal relative cooling power. From an applied viewpoint, these results demonstrate that the magnetocaloric response of metallic Shastry–Sutherland magnets can be tuned by adjusting the electron density, e.g., through chemical substitution. Overall, these findings confirmed that the oscillatory, long-range 2D RKKY interaction governs not only the

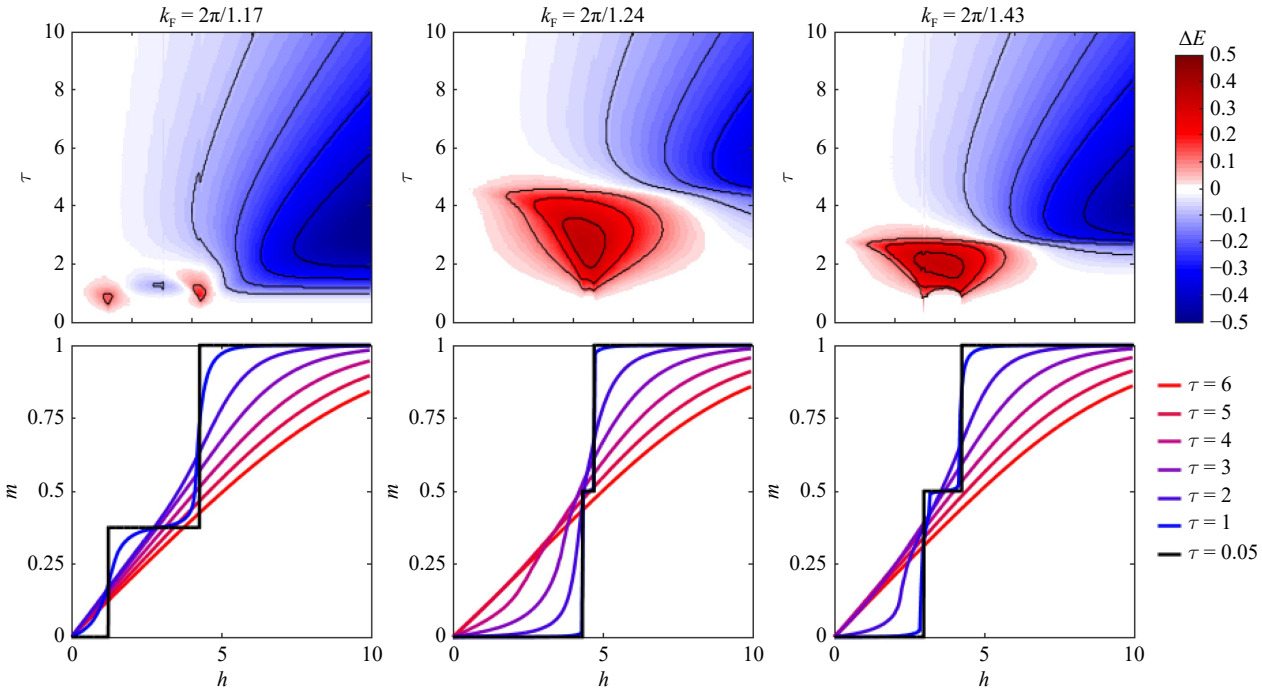

Fig. 6 Field dependence of the adiabatic entropy change $\Delta S(T, h)$ and the magnetization curves at different temperatures for several values of k_F in the two-dimensional Ising model on the SSL with the 2D RKKY interaction [75]. Alternating positive and negative peaks of ΔS indicate heating and cooling regions near metamagnetic transitions, while variations of k_F (electron and hole doping) shift the characteristic features and define optimal regimes for magnetocaloric performance.

magnetic ordering but also the field-induced entropy variations underlying the magnetocaloric effect. Because the coupling depends explicitly on the Fermi momentum, tuning the carrier concentration by doping provides a direct microscopic route to control and optimize the magnetocaloric response of metallic Shastry–Sutherland magnets.

3 Explicit inclusion of electrons: Spin–electron models on the Shastry–Sutherland lattice

While the RKKY framework successfully captures the indirect influence of conduction electrons on the localized magnetic moments, a more complete microscopic description requires the electrons to be treated as explicit quantum degrees of freedom. Such an approach allows one to analyse not only the effective magnetic coupling mediated by the electron gas, but also the feedback of the magnetic background on the itinerant subsystem itself. In metallic Shastry–Sutherland compounds this feedback manifests through the interplay between electron mobility, spin ordering, and Coulomb correlations, which jointly determine both the magnetization process and the magnetocaloric response.

The spin–electron model provides a natural framework to study these effects. It consists of itinerant electrons hopping between nearest-neighbour sites of the SSL and interacting locally with the Ising-type spins via the exchange coupling J_z. By systematically extending this minimal model to include electron–electron repulsion U, external magnetic field h, and later its classical-Ising reduction, represented by the so-called coupled double-Ising (CDI) model, one obtains a unified picture connecting localized and itinerant limits. The following subsections summarise a series of theoretical studies that progressively develop this approach, from the simplest models without Coulomb interaction, through correlated variants with finite U, to the full spin–electron model and its CDI representation, highlighting their thermodynamic and magnetocaloric properties in relation to the experimental behaviour of the rare-earth tetraborides.

3.1 Spin-electron coupling without Coulomb interaction

A microscopic description of the magnetization processes in metallic rare-earth tetraborides requires explicit inclusion of itinerant electrons rather than treating them only as mediators of effective interactions. The first comprehensive analysis of this kind was carried out in Ref. [76], where the authors introduced a minimal spin–electron model on the SSL and demonstrated that itinerant degrees of freedom are essential for reproducing the rich hierarchy of magnetization plateaus characteristic of these materials. A complementary finite-temperature study based on the same model was later presented in

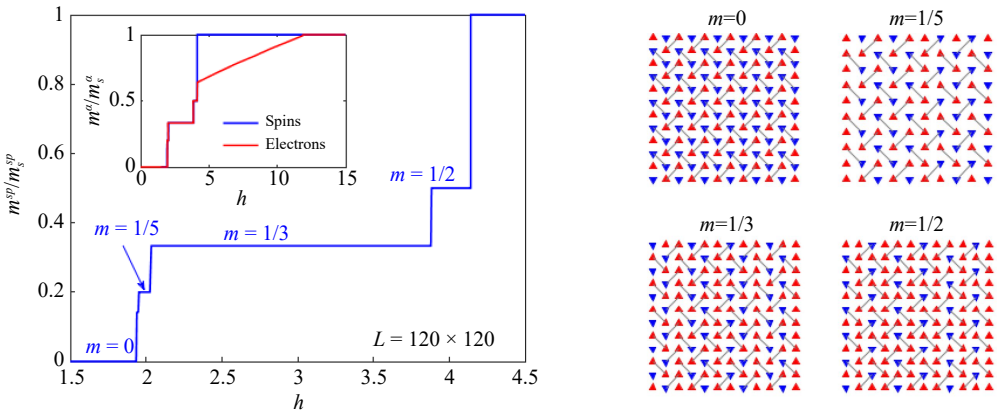

Fig. 7 Representative stripe configurations and magnetization curve of the spin–electron model (4) calculated for $J_1/J_2 = 1$, $J_z = 4$, $t_1 = 4$, $t_2 = 0.4t_1$. Reproduced from Ref. [76].

Ref. [77].

In the spin–electron model the conduction electrons hop between nearest- and next-nearest neighbour sites of the SSL, while localized magnetic moments are represented by Ising spins $S_i^z = \pm 1$. The electrons couple locally to these spins through an anisotropic Ising-type exchange interaction J_z, and an external magnetic field h acts on both the electron and spin subsystems. The Hamiltonian reads

$$\begin{aligned} H_0 = {} & t_1 \sum_{\langle ij\rangle\sigma} d_{i\sigma}^{\dagger} d_{j\sigma} + t_2 \sum_{\langle\langle ij\rangle\rangle\sigma} d_{i\sigma}^{\dagger} d_{j\sigma} \\ & + J_z \sum_i (n_{i\uparrow} - n_{i\downarrow}) S_i^z - h \sum_i (n_{i\uparrow} - n_{i\downarrow}) \\ & + J_1 \sum_{\langle ij\rangle} S_i^z S_j^z + J_2 \sum_{\langle\langle ij\rangle\rangle} S_i^z S_j^z - h \sum_i S_i^z, \end{aligned} \tag{4}$$

where $d_{i\sigma}^{\dagger}$ ($d_{i\sigma}$) creates (annihilates) an electron of spin σ at site i, and $n_{i\sigma} = d_{i\sigma}^{\dagger} d_{i\sigma}$. The parameters t_1 and t_2 denote the hopping amplitudes between nearest-neighbour $\langle ij\rangle$ and next-nearest-neighbour $\langle\langle ij\rangle\rangle$ sites of the Shastry–Sutherland lattice, respectively, while J_1 and J_2 are the corresponding antiferromagnetic Ising exchange couplings between localized spins. The model described by (4) is a direct generalization of the model introduced by Lemanski [87] that has been used later for the study of various cooperative phenomena in interacting spin–electron systems [88–91].

For a fixed Ising background $\{S_i^z\}$, the electronic part of the Hamiltonian is quadratic and can be diagonalized exactly. The total energy for a given configuration is obtained by filling the lowest N one-electron levels according to the prescribed electron number. The ground state at each magnetic field h is found by iteratively modifying the spin configuration and accepting any update that lowers the total energy. This hybrid scheme, described in detail in Ref. [92], combining exact diagonalization of the electronic subsystem with classical energy minimization for the localized spins, was applied to very large clusters up to 120×120 sites [76]. As a result, finite-size effects in the magnetization curve were strongly suppressed and even narrow plateau regions became visible.

The principal finding of Ref. [76] is that the interplay between electron hopping and spin–electron coupling stabilizes a series of commensurate magnetization plateaus at $m/m_s = 1/2$, $1/3$, $1/5$ on the $L = 120 \times 120$ cluster as well as $1/7$, $1/9$, $1/11$ plateaus on the $L = 140 \times 140$, 90×90 and 110×110 clusters, where m_s is the saturated magnetization of the localized spins. This sequence is much richer than that of the pure Ising SSL, which supports only the $1/3$ plateau. The plateaus at $1/2$, $1/3$, $1/5$, and $1/7$ appear as robust, finite intervals of the applied field, while those at $1/9$ and $1/11$ are narrower but clearly resolvable on sufficiently large clusters. Importantly, the calculated sequence closely mirrors the experimental hierarchy of plateaus in TmB_4, where plateaus at $1/7$, $1/8$, $1/9$, and $1/11$ precede a dominant $1/2$ step.

The microscopic origin of these plateaus is a family of stripe-like ground states formed by the localized spins. The system organizes into parallel antiferromagnetic (AF) bands of even width w separated by fully polarized ferromagnetic (FM) stripes. The value of w uniquely determines the magnetization $w = 1 \Rightarrow m/m_s = 1/2$, $w = 2 \Rightarrow m/m_s = 1/3$, $w = 4 \Rightarrow m/m_s = 1/5$, $w = 6 \Rightarrow m/m_s = 1/7$ with larger even values ($w = 8, 10$) yielding the fractions $1/9$ and $1/11$. These stripe textures minimize the combined kinetic and magnetic energies: electrons gain kinetic energy in the FM regions (where their motion is less restricted), while AF bands lower the frustrated Ising exchange energy. The resulting commensurate AF/FM patterns represent the compromise that optimizes the total energy at each applied field. Representative stripe patterns for the major plateaus, together with the corresponding magnetization curve, are shown in Fig. 7.

The behaviour of the itinerant electrons reflects the

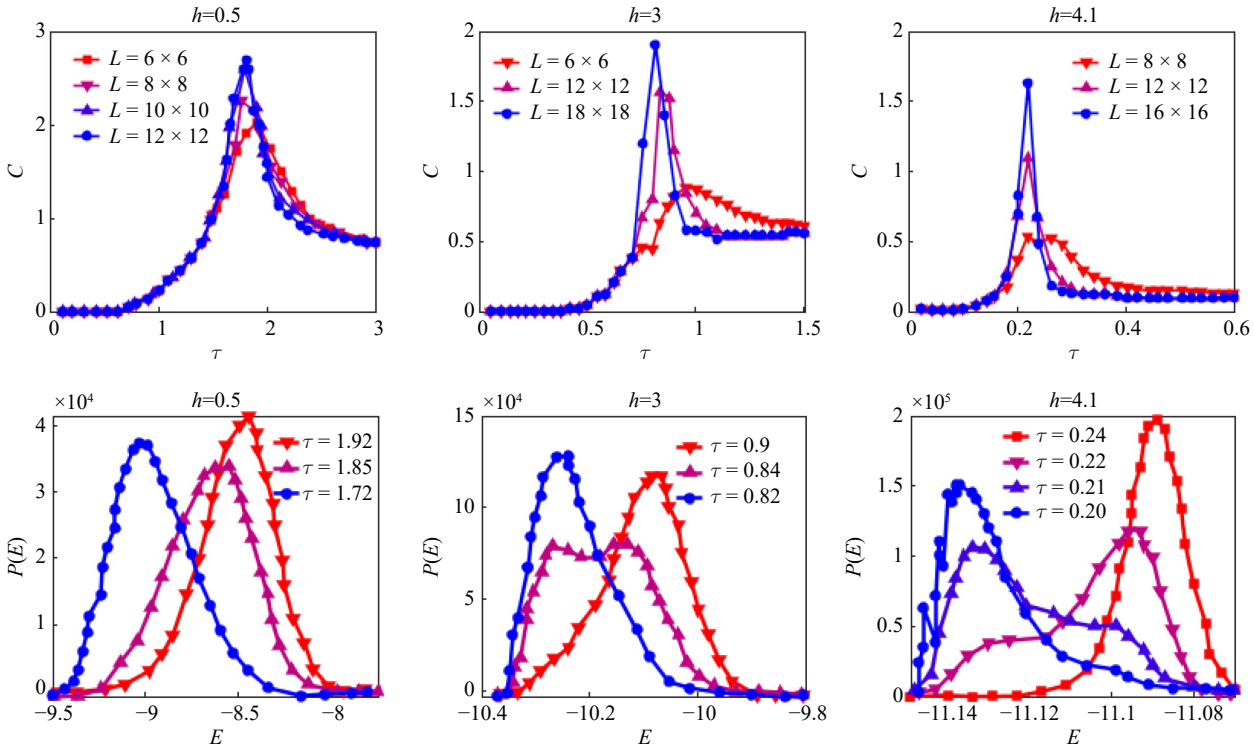

Fig. 8 Finite-temperature behaviour of plateau phases: specific heat C, and energy distributions $P(E)$ used to distinguish first- and second-order transitions. Reproduced from Ref. [77].

spin textures. For $m/m_s \leq 1/2$, the electron magnetization follows the localized spins closely, especially when J_z is large. In AF bands, electrons experience alternating local fields and reduced mobility, while in FM stripes their spectrum broadens. For $m/m_s > 1/2$, the spins saturate rapidly, but the electrons polarize more gradually, consistent with the persistence of itinerant character even in high magnetic fields.

The finite-temperature stability of the stripe phases was analyzed in Ref. [77] using canonical Monte Carlo simulations on SSL clusters up to 18×18 sites. For representative fields corresponding to $m/m_s = 0$, $1/3$, and $1/2$, pronounced peaks in the specific heat signal thermal transitions from the low-temperature ordered phases to a disordered paramagnetic state. The transition temperatures depend strongly on the magnetization fraction: the AF ground state ($m = 0$) melts at a relatively high reduced temperature $\tau_c \approx 1.8$; the $1/3$ stripe phase melts at roughly half this value; and the $1/2$ plateau is stable only up to temperatures almost an order of magnitude smaller. These trends highlight the varying energetic cost of destroying AF regions of different widths and FM stripe patterns.

The nature of the thermal transitions is revealed by the energy histograms $P(E)$ near τ_c. For $m/m_s = 0$ and $m/m_s = 1/2$, $P(E)$ remains single-peaked, which according to [93] indicates continuous second-order transitions. For the $1/3$ plateau, however, $P(E)$ becomes clearly double-peaked, consistent with a first-order transition and coexistence of ordered and disordered states. Representative specific-heat curves, and energy histograms are shown in Fig. 8.

Taken together, these results demonstrate that the $U = 0$ spin–electron model on the SSL provides a minimal but remarkably accurate microscopic description of the magnetization processes in metallic rare-earth tetraborides. It reproduces the major plateaus at $1/3$ and $1/2$ as well as the smaller fractional ones at $1/5$, $1/7$, $1/9$, and $1/11$, and it captures their finite-temperature behaviour and transition orders. The explicit treatment of itinerant electrons is thus essential for understanding the experimentally observed hierarchy of fractional magnetization plateaus and the thermal properties of these highly frustrated magnetic metals.

3.2 Electron–electron correlation and anisotropic exchange effects

While the spin–electron coupling in the $U = 0$ model already reproduces a hierarchy of fractional magnetization plateaus, the experimentally observed behaviour of metallic rare-earth tetraborides requires several additional microscopic ingredients. In particular, many RB_4 compounds display a dominant and very robust $1/2$ plateau, whereas the $1/3$ plateau is strongly reduced or even entirely absent, as in ErB_4 and TmB_4. The minimal

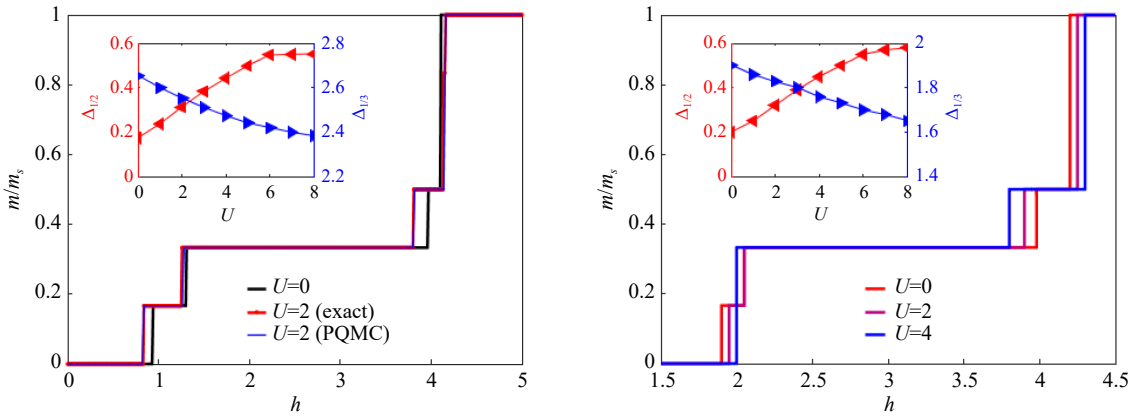

Fig. 9 Magnetization curves of the spin–electron model (5) on the $L = 12$ (left) and $L = 12 \times 12$ (right) cluster and different values of U. The inset shows the width of the 1/2 and 1/3 plateau as a function of the Coulomb interaction U. Reproduced from Ref. [78].

Ising-type spin–electron model is not sufficient to account for this imbalance, and therefore two natural generalizations have been introduced and analysed in Refs. [78, 79]: on-site electron–electron repulsion of the Hubbard type, and anisotropic exchange interactions that include both local double-exchange processes and transverse Heisenberg terms. These two extensions modify the stability competition between the 1/3 and 1/2 plateau phases in qualitatively different but complementary ways.

The first extension incorporates the Hubbard interaction into the spin–electron Hamiltonian, adding a term that penalizes double occupancy on each site. The resulting model takes the form

$$H_U = H_0 + U \sum_i n_{i\uparrow} n_{i\downarrow}, \tag{5}$$

where H_0 is given by Eq. (4) (with $J_1 = J_2$ and $t_1 = t_2$). The inclusion of U makes the electronic subsystem interacting, necessitating the use of exact diagonalization [94] for $L = 12$ Betts cluster [95, 96] and the Projector Quantum Monte Carlo method [97–99] for clusters of size 12×12. These calculations reveal a clear and systematic trend [78]: electron–electron correlations strongly suppress the 1/3 plateau and simultaneously stabilize and widen the 1/2 plateau. Even moderate values such as $U = 2$ increase the width of the 1/2 plateau by roughly a factor of three, while the 1/3 plateau shrinks steadily with increasing U, but it is still much larger than that of the 1/2 plateau. The agreement between ED and PQMC results indicates that these effects persist in the thermodynamic limit.

From a microscopic perspective, the Hubbard term disfavors the formation of narrow antiferromagnetic regions that underlie the 1/3 plateau, since these tend to localize electrons in environments prone to double occupancy. The 1/2 plateau, based on a wider commensurate AF–FM stripe pattern, is energetically more favourable when correlated electrons must avoid double occupancy. This mechanism naturally explains why many RB_4 compounds show a very broad and dominant 1/2 plateau, whereas the 1/3 plateau is suppressed or completely absent. Representative magnetization curves demonstrating the correlation-induced disappearance of the 1/3 plateau and simultaneous enhancement of the 1/2 plateau are shown in Fig. 9.

A second extension was developed in Ref. [79], motivated by the observation that real RB_4 magnets exhibit finite transverse components of both the local d–f exchange and the $4f$–$4f$ interaction. These transverse couplings introduce spin-flip terms into the Hamiltonian and modify the balance between the competing plateau phases even in the absence of Hubbard interaction. The extended spin–electron Hamiltonian becomes

$$\begin{aligned} H = H_U &+ 2J_{xy} \sum_i (d^\dagger_{i\uparrow} d_{i\downarrow} f^\dagger_{i\downarrow} f_{i\uparrow} + d^\dagger_{i\downarrow} d_{i\uparrow} f^\dagger_{i\uparrow} f_{i\downarrow}) \\ &+ J'_{xy} \sum_{\langle ij \rangle} (f^\dagger_{i\uparrow} f_{i\downarrow} f^\dagger_{j\downarrow} f_{j\uparrow} + f^\dagger_{i\downarrow} f_{i\uparrow} f^\dagger_{j\uparrow} f_{j\downarrow}) \\ &+ J'_{xy} \sum_{\langle\langle ij \rangle\rangle} (f^\dagger_{i\uparrow} f_{i\downarrow} f^\dagger_{j\downarrow} f_{j\uparrow} + f^\dagger_{i\downarrow} f_{i\uparrow} f^\dagger_{j\uparrow} f_{j\downarrow}), \end{aligned} \tag{6}$$

where H_U is given by Eq. (5) and in accordance with the geometry of the SSL in RB_4 compounds, the same value of the transverse Heisenberg exchange term J'_{xy} is assumed for nearest- and next-nearest-neighbour spins. Exact Lanczos and truncated Lanczos calculations on $L = 12$ and $L = 36$ clusters show that the two transverse exchange parameters have completely opposite effects on the magnetization process. The on-site double-exchange term J_{xy} tends to destroy the 1/2 plateau and stabilizes the 1/3 plateau; once J_{xy} exceeds approximately $J_z/2$, the 1/2 plateau disappears altogether, while the 1/3 plateau remains present up to the isotropic limit $J_{xy} = J_z$. In contrast, the transverse Heisenberg term J'_{xy} stabilizes the 1/2 plateau and suppresses the 1/3

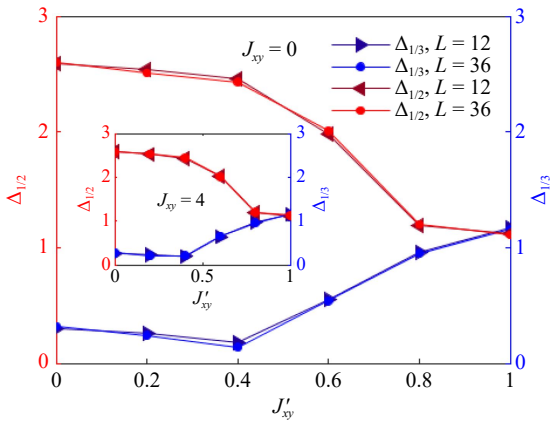

Fig. 10 The width of the 1/2 and 1/3 plateau as a function of J'_{xy} calculated by the Lanczos ($L = 12$) and truncated Lanczos ($L = 36$) method for $J_{xy} = 0$ and $J_{xy} = 4$ (inset) of the anisotropic-exchange model (6) from Ref. [79].

plateau: for $J'_{xy} > 0.4$, the width of the 1/3 plateau is reduced by a factor of nearly 2.5, while the width of the 1/2 plateau increases by a factor of about 3.5 compared to the purely Ising case.

Consequently, the transverse exchange parameters provide two distinct microscopic routes for tuning the 1/3–1/2 plateau competition. The double-exchange term weakens the stripe patterns with wide antiferromagnetic regions characteristic of the 1/2 plateau, whereas the transverse Heisenberg interaction strengthens exactly those configurations. In materials with strong Ising anisotropy ($J_{xy}, J'_{xy} \ll J_z$) the double-exchange term is relatively unimportant, but even small J'_{xy} can substantially modify the plateau widths. This observation highlights the need to include transverse $4f$–$4f$ exchange when modelling RB_4 magnets and simultaneously explains why the simplified Ising spin–electron model remains valid when these transverse terms are weak. Representative magnetization curves showing these opposite effects of J_{xy} and J'_{xy} are presented in Fig. 10.

In summary, electron–electron correlations and anisotropic exchange processes represent two independent mechanisms that both drive the system toward the experimentally observed dominance of the 1/2 plateau and suppression of the 1/3 plateau. The Hubbard interaction disfavors the narrow antiferromagnetic bands that stabilize the 1/3 plateau, while the transverse Heisenberg exchange directly strengthens the stripe structure responsible for the 1/2 plateau. Together, these effects significantly improve the agreement between theoretical predictions and the magnetization curves of metallic rare-earth tetraborides.

3.3 Full correlated spin–electron model and CDI mapping

In the previous subsection we have discussed the influence of electron-electron correlations and anisotropic exchange couplings within the spin–electron framework. The next natural step towards a complete and realistic description of metallic Shastry–Sutherland magnets is to introduce the real spin values of both subsystems, corresponding to the $4f$ ions ($S = 1, 3/2, 2$) and itinerant $5d$ electrons ($s_d = 1/2$), and to examine how this mixed-spin structure modifies the ground-state and thermodynamic properties. This generalization, first analysed in Ref. [80], provided the foundation for a systematic mapping to the effective CDI model [81], which allowed one to study much larger clusters and to explore finite-temperature effects including the magnetocaloric response [82].

To model realistically the situation in rare-earth tetraborides, the localized spins $S_i^z = \pm S$ are assigned the real spin values corresponding to the magnetic ions Ho^{3+} ($S = 2$), Er^{3+} ($S = 3/2$) and Tm^{3+} ($S = 1$), while the itinerant d electrons possess the spin $s_d = 1/2$. The spin subsystem is described by the Ising interaction between the first- (J_1) and second-nearest (J_2) neighbours, whereas the itinerant electrons are governed by the Hubbard Hamiltonian with on-site Coulomb repulsion U. Both subsystems are coupled through an anisotropic Ising-type interaction J_z, and the magnetic field h acts on the spins and electrons separately. Thus, the mixed-spin Hamiltonian is formally identical to the one discussed in the previous section [Eq. (5)], the only modification being the use of realistic spin values for the localized magnetic moments and itinerant electrons. In the next, the case $J_1 = J_2$ and $t_1 = t_2$ is considered, corresponding to identical coupling/hopping amplitudes along the square and diagonal bonds of the Shastry–Sutherland lattice.

Using exact diagonalization on the Betts cluster ($L = 12$ sites) and the Projector Quantum Monte Carlo method on 6×6 lattices, the authors investigated how the Coulomb interaction U and the mixed-spin combinations affect magnetization processes. The resulting ground-state phase diagrams in the h–U plane (Fig. 11) show that for $S = 1$ and $S = 3/2$ the Coulomb interaction stabilizes the single macroscopic $m/m_s = 1/2$ plateau and suppresses the 1/3 plateau, in excellent agreement with the experimental magnetization curves of TmB_4 and ErB_4. For $S = 2$ (corresponding to HoB_4), the 1/2 plateau disappears and a different sequence with 1/3 and 7/15 plateaus is observed, again in accord with experiments.

Finite-temperature simulations (Fig. 12) further revealed that the specific heat capacity exhibits either a single-peaked or a double-peaked structure depending on the spin value S and the coupling J_z. The high-temperature peak originates from the spin subsystem, while the low-temperature peak arises from the itinerant electrons. For large U, the electron peak is shifted to very low temperatures (below 0.2 in reduced units), which

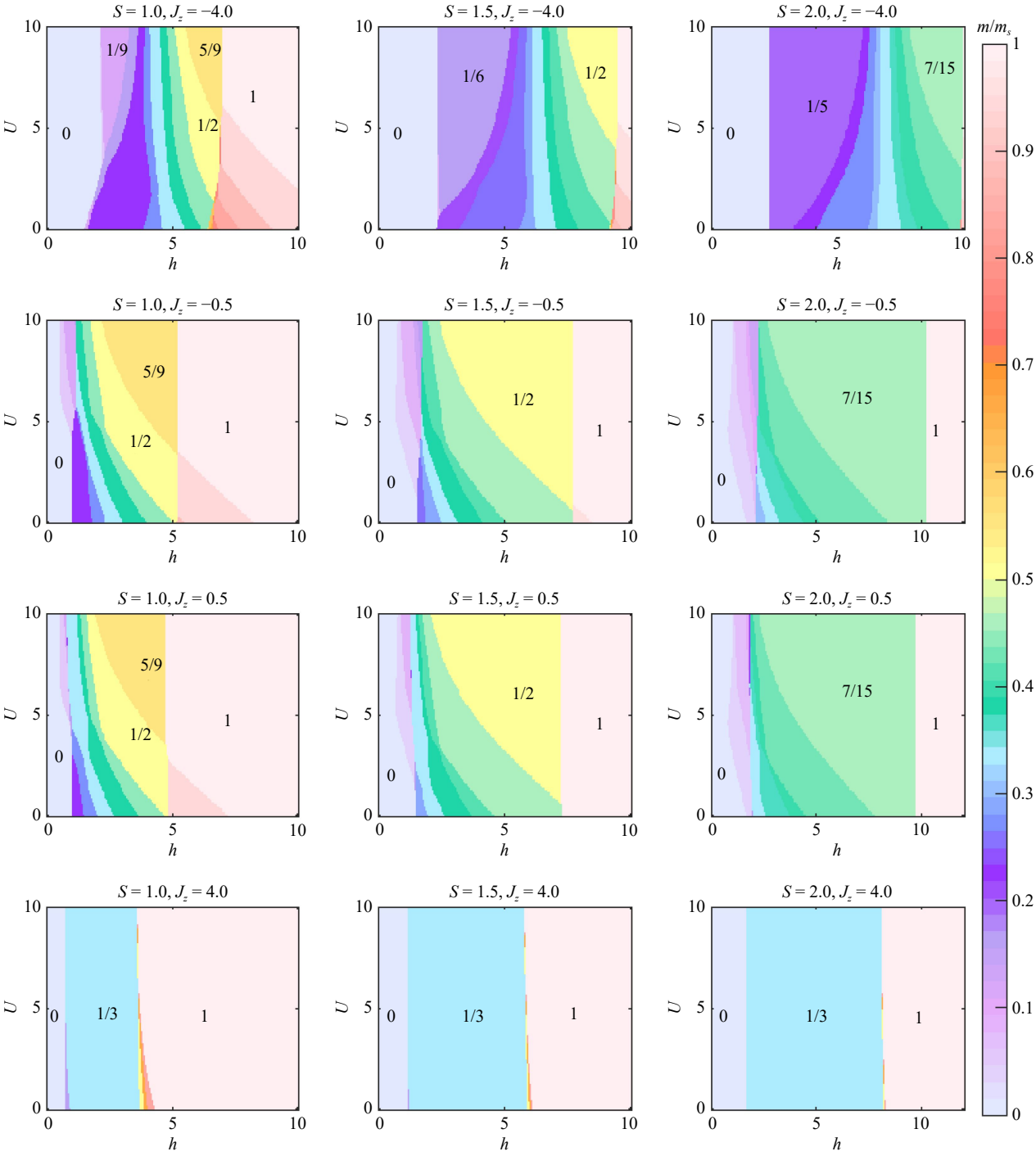

Fig. 11 Ground-state phase diagrams of the mixed-spin correlated spin–electron model in the h–U plane for $S = 1$, 3/2, and 2. Reproduced from [80].

explains why only the single high-temperature peak is detected experimentally, the lower electron contribution lies far below the 2 K range typically accessible in measurements.

The mixed-spin Hamiltonian is still fully quantum and numerically demanding. To overcome the size limitations, Ref. [81] introduced a mapping to the simpler CDI model valid under three physically realistic conditions: (i) the Coulomb interaction U between conduction electrons is large ($U \gg t$); (ii) the conduction band is half-filled ($n = 1$); and (iii) the system exhibits strong easy-axis anisotropy. Under these assumptions, the itinerant-electron subsystem described by the Hubbard model can be replaced by an effective Ising branch with coupling $J'_{ij} = 4t_{ij}^2/U$ [100], leading to the effective Hamiltonian

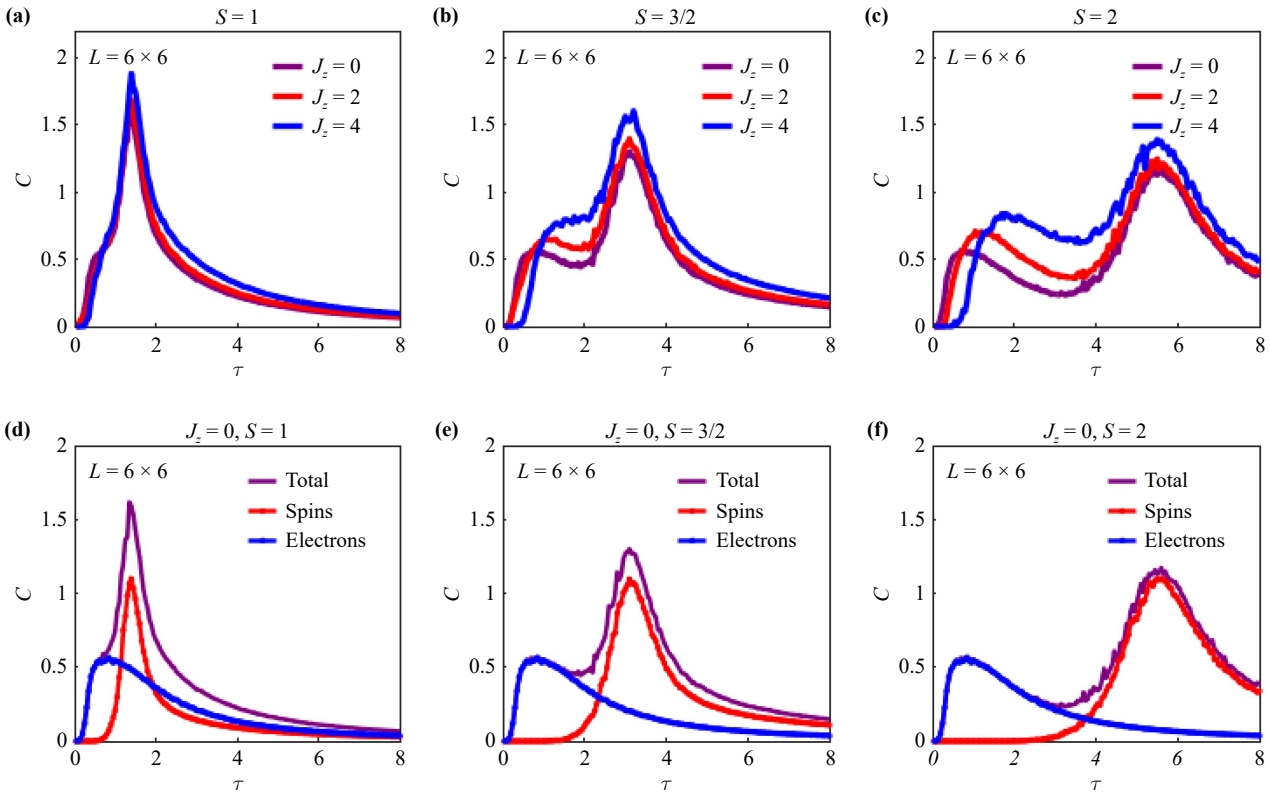

Fig. 12 Temperature dependence of the specific heat capacity at various J_z for the mixed-spin model from Ref. [80]. The high-temperature Ising peak originates from the spin subsystem, whereas the low-temperature electron peak corresponds to the itinerant electrons and is shifted to very low τ for large U.

$$H_{\mathrm{CDI}} = \sum_{ij} J_{ij} S_i^z S_j^z + \sum_{ij} J'_{ij} s_i^z s_j^z + J_z \sum_i s_i^z S_i^z - h \sum_i (S_i^z + s_i^z), \tag{7}$$

which describes two interacting Ising lattices: the spin branch (S_i^z) and the electron branch (s_i^z). The exchange couplings J_{ij} (J'_{ij}) correspond to the Ising interactions J_1 and J_2 (J'_1 and J'_2) acting on the nearest- and next-nearest neighbors of the Shastry–Sutherland lattice, respectively. In the following, these couplings are taken equal, $J_1 = J_2 = J$ ($J'_1 = J'_2 = J'$). The inter-branch coupling J_z can be ferromagnetic ($J_z < 0$) or antiferromagnetic ($J_z > 0$).

Extensive Monte Carlo simulations on clusters up to 60×60 sites demonstrated that the CDI model reproduces the essential physics of the full spin–electron Hamiltonian even for moderate J_z. The comparison of magnetization curves for both models (Fig. 13) shows nearly perfect coincidence in the strong-coupling regime.

The CDI model allows simulations on much larger clusters and thus reveals a richer hierarchy of magnetization plateaus. Depending on the parameters (J', J_z, S), several characteristic sequences appear, among which the dominant 1/2 plateau phase persists for $S = 1$ and 3/2 (TmB_4, ErB_4), while the 1/3 phase is strongly suppressed. For $S = 2$ (HoB_4), the 1/3 phase remains dominant, in full analogy with experiments.

Finite-temperature results for the CDI model reproduce the experimentally observed single high-temperature peak in the specific heat capacity and predict an additional low-temperature peak originating from the electron branch (Fig. 15). The latter is expected to occur below the temperature range accessible in experiments, which explains its absence in current data on TmB_4 and ErB_4.

The most recent extension of this framework [82] focused on the magnetocaloric properties of the CDI model. Using Monte Carlo simulations combined with the parallel-tempering technique, the field dependence of the isothermal entropy change $\Delta S(T,h) = S(T,h) - S(T,0)$ and the relative cooling power were computed for representative parameter sets corresponding to TmB_4 and ErB_4. The results (Fig. 16) reveal alternating positive and negative peaks of ΔS associated with successive metamagnetic transitions between fractional plateau states. The main cooling region is located near the transition between the low-field antiferromagnetic phase and the 1/2 plateau, where ΔS reaches its maximal magnitude. This alternating "heating-cooling" pattern of ΔS reproduces closely the experimental magnetocaloric behaviour of metallic Shastry–Sutherland compounds.

In summary, the full correlated spin–electron model

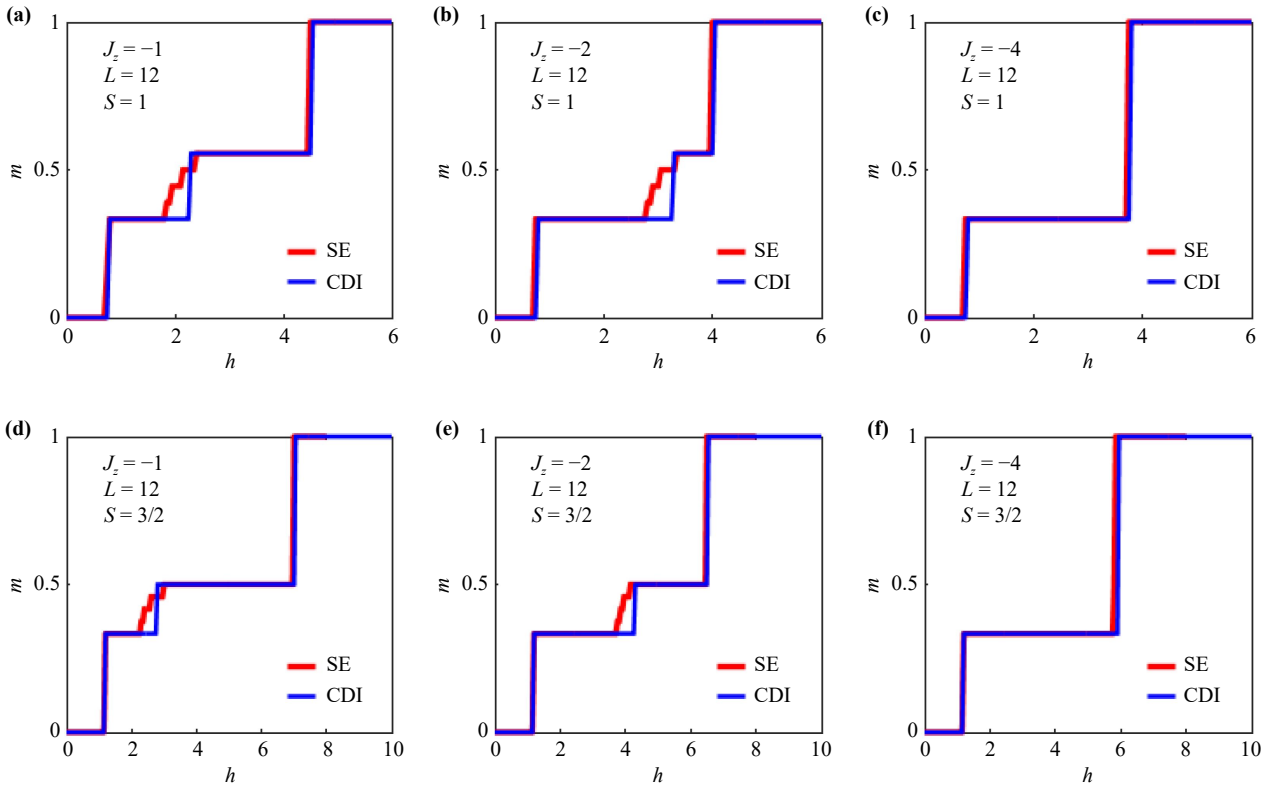

Fig. 13 Comparison of the total magnetization curves obtained from the full spin–electron model and the effective CDI model (after [81]). The near-perfect agreement confirms that the CDI model retains the relevant physics of the full Hamiltonian.

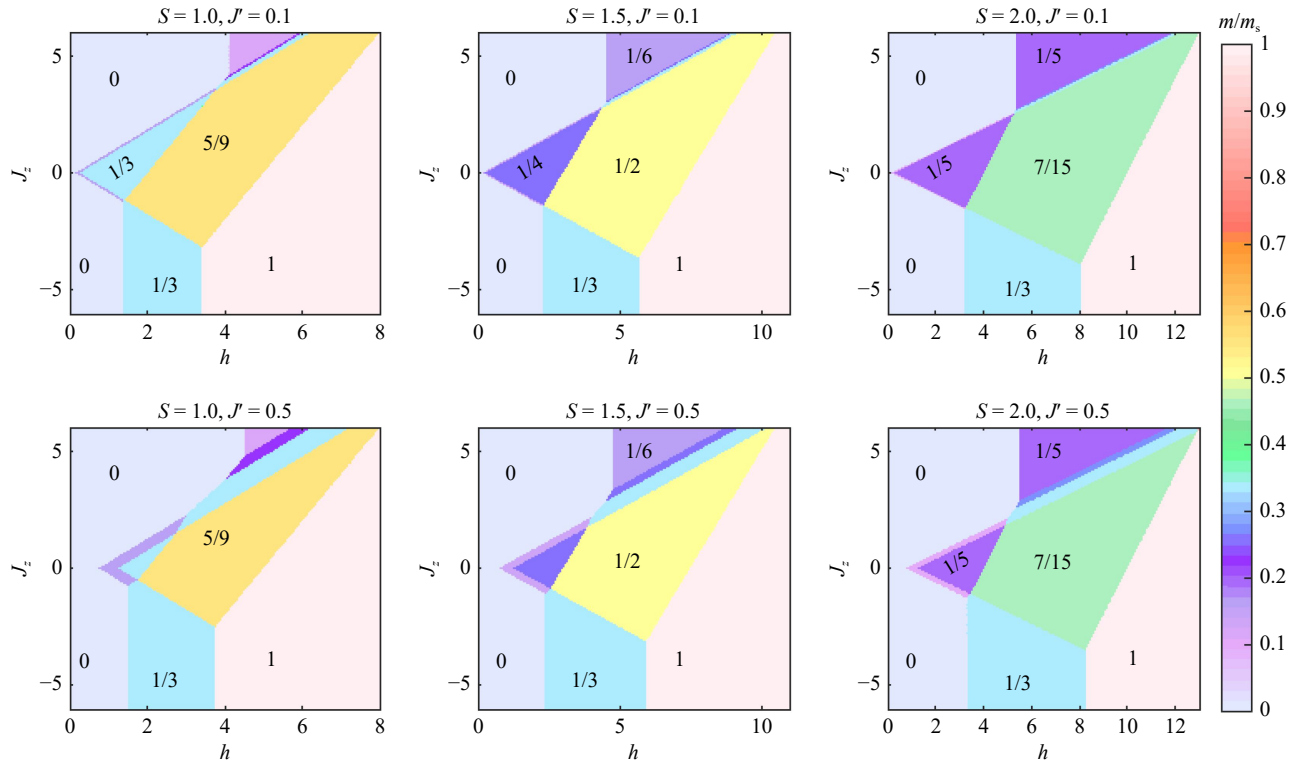

Fig. 14 Magnetic phase diagrams of the CDI model in the h–J_z plane for several values of spins S and interactions J' (after Ref. [81]).

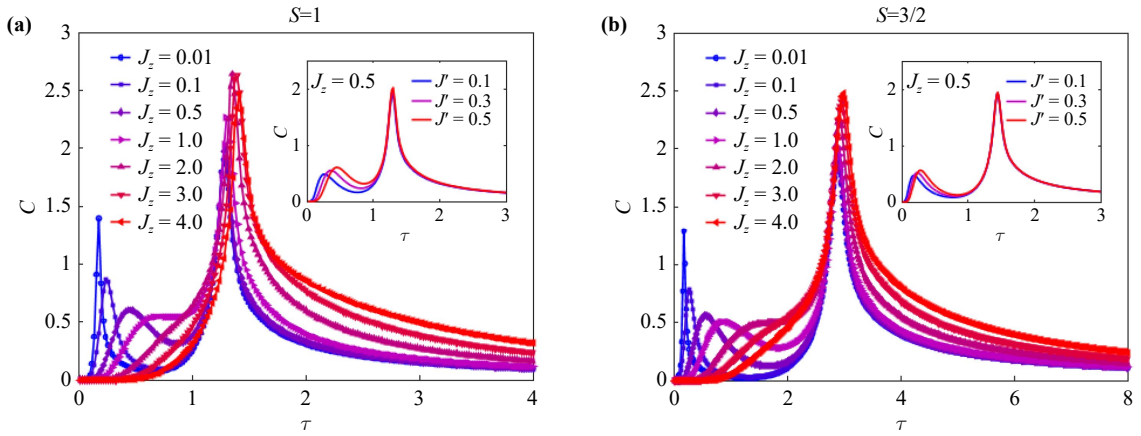

Fig. 15 Temperature dependence of the specific heat capacity of the CDI model for spins $S = 1$ **(a)** and $S = 3/2$ **(b)** from Ref. [81].

with realistic mixed spins and its mapping onto the coupled double-Ising model provide a unified microscopic framework capable of describing both the magnetic and thermodynamic properties of rare-earth tetraborides. The inclusion of real spin values and Coulomb correlations accounts for the material-dependent stabilization of magnetization plateaus, while the CDI representation enables large-scale simulations that reproduce experimental features of specific heat and magnetocaloric response. These results demonstrate that despite its relative simplicity, the CDI model retains the essential physics of the full spin–electron Hamiltonian and offers an efficient route for further studies of correlated spin-electron systems on frustrated lattices.

3.4 Impact of charge stripes on magnetization processes

The most recent development in the modelling of magnetization processes in rare-earth tetraborides is the inclusion of charge inhomogeneity, motivated by experimental observations of charge stripes in structurally related borides [101–106]. In Ref. [83] a phenomenological spatially varying local potential V_i was introduced into the spin–electron Hamiltonian to account for possible charge ordering arising from static or dynamic Jahn-Teller distortions of boron clusters, similar to those observed in rare-earth hexaborides [105] and dodecaborides [106]. Although the charge modulation is introduced here in an ad-hoc manner, similarly to some previous works [107–109] addressing related problems, its inclusion provides a microscopic description of the magnetization processes fully consistent with the experimental data for TmB_4 and ErB_4.

The total Hamiltonian was written as

$$H = H_0 + \sum_{i,\sigma} V_i n_{i\sigma}, \tag{8}$$

where H_0 denotes the conventional spin-electron model on the Shastry–Sutherland lattice given by Eq. (4). The term with V_i represents a periodic modulation of the local electronic potential and generates different types of charge stripes. The model was solved using an exact-diagonalization-based numerical scheme on $L = 6 \times 6$ and 12×12 clusters for all nonequivalent periodic potentials up to period $p=4$.

The calculations revealed that the form and intensity of the potential V_i have a dramatic impact on the stability of individual magnetization plateaus. Among all 1798 periodic potentials examined on the 6×6 cluster, the strongest effect was found for the configuration composed of full axial charge stripes alternating with chessboard stripes (Fig. 17). This pattern enhances the $m/m_s = 1/2$ plateau and simultaneously suppresses the 1/3 plateau, leading to a very simple magnetization curve containing only these two main fractional plateaus and the zero-field phase. The enlargement of the 1/2 plateau and the reduction of the 1/3 plateau become more pronounced with increasing amplitude V and spin–electron coupling J_z.

Further tests on larger 12×12 clusters confirmed the robustness of this result. Two symmetry-inequivalent variants of the stripe potential, denoted $V_i^{(1)}$ and $V_i^{(2)}$, were analysed (Fig. 18). Both produce nearly identical magnetization curves dominated by the 1/2 plateau and show complete suppression of the 1/3 plateau for large V. The ground-state spin configuration within the 1/2 phase is commensurate with the stripe pattern and coincides with the magnetic structure experimentally observed in TmB_4.

The calculated local electron occupations $n_i = \langle n_{i\uparrow} + n_{i\downarrow} \rangle$ demonstrate that increasing V induces a strong modulation of the electronic density, producing alternating fully and partially occupied stripes analogous to the conducting channels observed in CeB_6 and LuB_{12}. This commensurability between charge and spin order provides a natural microscopic explanation for the

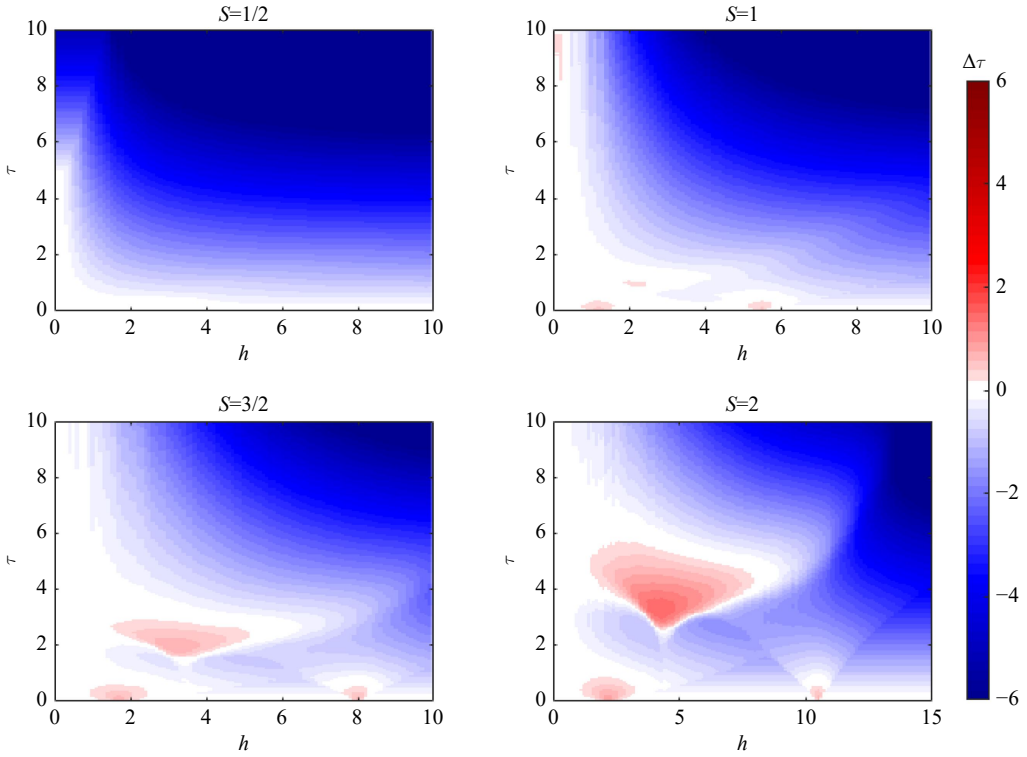

Fig. 16 Field dependence of the isothermal entropy change $\Delta S(T,h)$ in the CDI model (after [82]). Alternating positive and negative peaks correspond to heating and cooling regions near metamagnetic transitions between fractional plateau states.

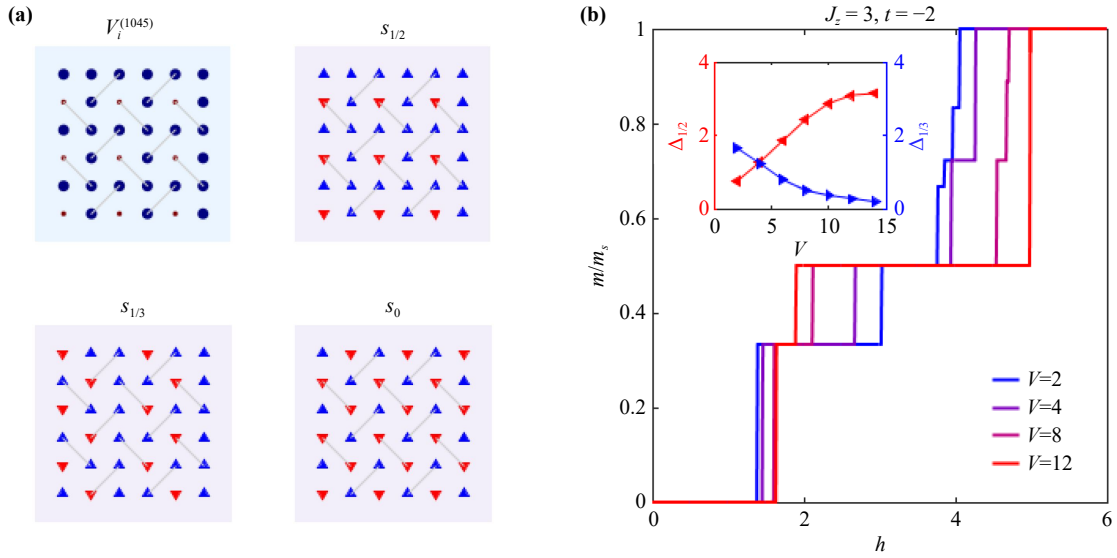

Fig. 17 **(a)** Spatial form of the local potential $V_i^{(1045)}$ corresponding to the mixed stripe pattern and ground-state spin configurations s_0, $s_{1/3}$ and $s_{1/2}$. **(b)** Magnetization curves calculated for $J_z = 3$, $t = -2$, and different potential amplitudes V (after [83]).

robust 1/2 plateau and the disappearance of the 1/3 phase in TmB_4 and ErB_4.

To quantify the comparative efficiency of different theoretical models in stabilizing the 1/2 plateau, Ref. [83] evaluated the ratio $\Delta_{1/2}/\Delta_{1/3}$ of the plateau widths for several representative frameworks (see Table 1). The spin-electron model with charge stripes (SEM+ChS) achieved $\Delta_{1/2}/\Delta_{1/3} \to \infty$, outperforming all previous models including the Ising (0), anisotropic Heisenberg (0.46), Ising+J_3 (0.67), Ising+RKKY (1.86), and correlated

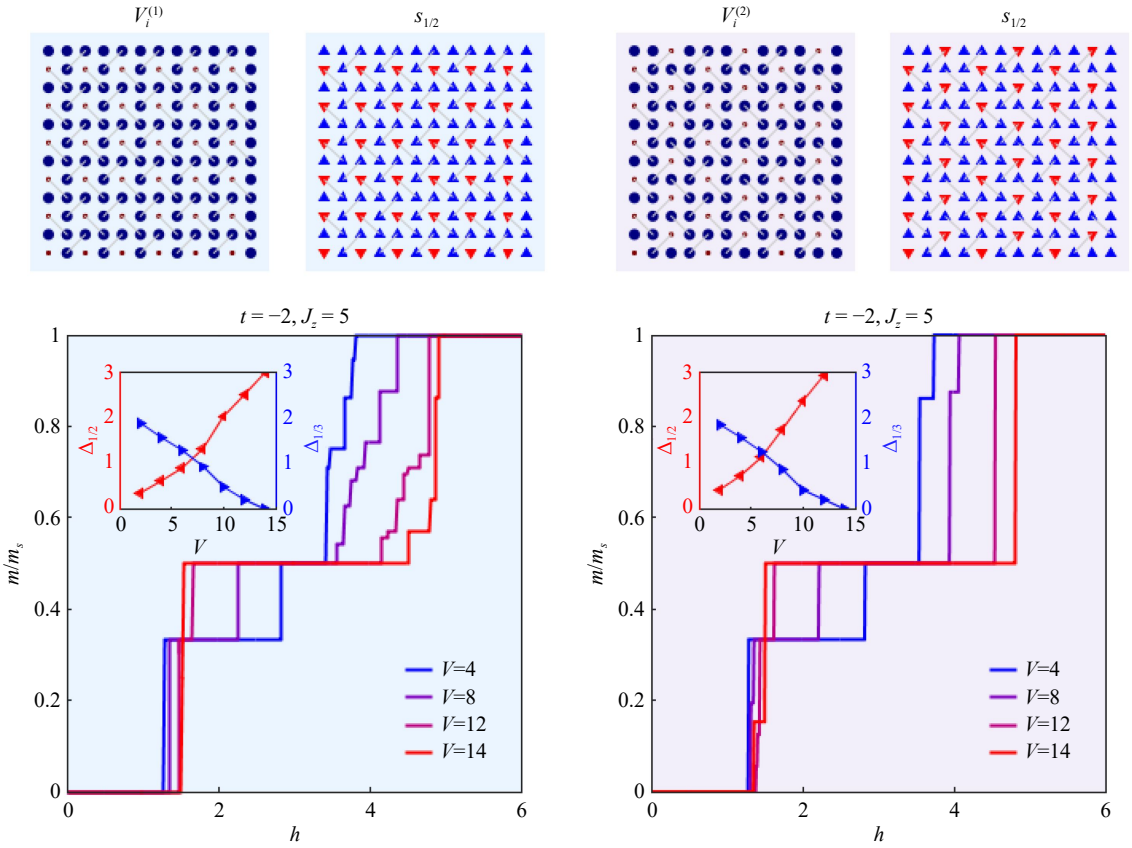

Fig. 18 Magnetization curves, widths of the 1/2 and 1/3 plateaus, and spin configurations $s_{1/2}$ corresponding to two stripe potentials $V_i^{(1)}$ and $V_i^{(2)}$ on the 12×12 cluster (after [83]).

Table 1 Optimal $\Delta_{1/2}/\Delta_{1/3}$ ratios for representative models.

Model	$\Delta_{1/2}/\Delta_{1/3}$	Ref.
Ising model (IM)	0.00	[60, 61]
Anisotropic Heisenberg model (AHM)	0.46	[59]
Ising + J_3 interaction (IM+J_3)	0.67	[66, 67]
Ising + RKKY interaction (IM+RKKY)	1.86	[72]
Spin–electron model (SEM)	0.14	[76]
SEM + Coulomb U (SEM+U)	0.47	[78]
SEM + charge stripes (SEM+ChS)	∞	[83]

spin–electron (0.47) models.

In conclusion, the introduction of charge stripes into the spin–electron framework yields a minimal and robust mechanism for the complete suppression of the 1/3 plateau and stabilization of the 1/2 plateau over a broad parameter range. The resulting magnetization curves reproduce the experimental behaviour of TmB_4 and ErB_4 without invoking long-range or higher-order interactions. Although the local potential V_i is phenomenological, its success suggests that intrinsic charge modulations – possibly driven by Jahn–Teller distortions of boron clusters – may indeed be the missing ingredient governing the magnetization processes in the rare-earth tetraborides.

4 Conclusion

The theoretical description of magnetization processes and thermodynamic behaviour in rare-earth tetraborides represents a uniquely challenging problem, combining strong geometrical frustration, itinerant-electron effects, long-range interactions, and material-specific anisotropies. In this review we have traced the evolution of theoretical approaches from the earliest Ising-type descriptions on the Shastry–Sutherland lattice to progressively more realistic formulations that incorporate indirect RKKY exchange, explicit spin–electron coupling, on-site electron correlations, transverse exchange terms, mixed-spin generalizations, and the

influence of charge inhomogeneity. Taken together, these studies now provide a coherent microscopic picture capable of explaining the experimentally observed hierarchy of fractional magnetization plateaus, the dominance of the half-magnetization state in several members of the RB_4 family, and the unusual magnetocaloric signatures characteristic of these metallic frustrated magnets.

The RKKY-based models represent the first major step beyond purely localized spin descriptions. Their significance lies in providing a direct microscopic origin for the longer-range competing interactions that were formerly introduced ad hoc into classical Ising Hamiltonians. By expressing the exchange integrals in terms of the Fermi momentum of conduction electrons, the RKKY framework establishes an explicit connection between electronic structure and magnetic ordering. The early work of Feng *et al.* demonstrated that even the simplest 3D RKKY form is capable of stabilizing the experimentally dominant 1/2 plateau in TmB_4. Subsequent refinements by Regeciová and Farkašovský revealed a far richer landscape: when realistic simulation sizes, parallel tempering, and mixed 3D–2D approximations are used, the RKKY interaction produces not only the 1/2 plateau, but also a cascade of fractional plateaus (1/3, 3/8, 7/18, $\cdots$) and a dense sequence of ferrimagnetic superstructures. The 2D RKKY formulation highlighted the role of electronic dimensionality by simplifying the magnetization curve into essentially a single robust 1/2 plateau with few subsidiary steps, closely reproducing the behaviour of ErB_4. In contrast, the fully 3D RKKY model gave rise to a hierarchical sequence of commensurate phases remarkably similar to those observed in TmB_4 and TbB_4, including the elusive 1/8 plateau. These findings collectively demonstrate that the oscillatory, long-range, Fermi-surface-controlled character of the RKKY interaction is a fundamental ingredient in understanding why different RB_4 compounds display different plateau sequences. They also highlight the microscopic sensitivity of the magnetic phase diagram to the carrier concentration, explaining why doping produces pronounced modifications of plateau stability and critical fields.

Despite the success of the indirect-electron approaches, their inability to describe the feedback of the magnetic background on the itinerant subsystem represents a conceptual limitation. Explicit spin-electron models overcome this difficulty by treating the conduction electrons as active quantum degrees of freedom coupled locally to the Ising-like rare-earth moments. The simplest $U = 0$ model already produces a strikingly realistic hierarchy of magnetization plateaus, including 1/2, 1/3, 1/5, 1/7, 1/9 and 1/11, with the correct stripe-type magnetic textures. The fact that these structures emerge solely from the competition between electron hopping and local spin–electron coupling is of fundamental importance: it shows that commensurate AF–FM superstructures in RB_4 are not artifacts of long-range exchange, but intrinsic patterns favored by itinerant electrons on the frustrated SSL. The follow-up finite-temperature study clarified the thermodynamic stability of these plateaus and established that the melting of the 1/3 plateau is first-order while the 1/2 plateau melts continuously at much lower temperatures. This dichotomy naturally reflects the different widths of the AF bands underlying each plateau, reinforcing the view that the stripe geometry is the microscopic key to plateau formation.

The inclusion of electron–electron correlations represents another crucial milestone. The correlated spin-electron model with a finite Hubbard interaction revealed an especially important result: electron correlations strongly stabilize the 1/2 plateau and suppress the 1/3 plateau. Even moderate repulsion enhances the energetic cost of narrow AF regions and therefore penalizes the 1/3 stripes, while broadening and strengthening the 1/2 plateau. This provides a compelling and microscopically grounded explanation for the behaviour of ErB_4 and TmB_4, where the 1/3 plateau is absent or extremely narrow and the magnetization curve is dominated by the half-magnetization state. Notably, this conclusion emerges independently of the RKKY mechanism and demonstrates that electron correlations alone can drive the system toward experimentally observed plateau structures.

The model incorporating transverse exchange terms (J_{xy} and J'_{xy}) revealed a complementary and equally enlightening perspective. The local double-exchange process J_{xy} destabilizes the 1/2 plateau while favouring the 1/3 plateau, whereas the transverse Heisenberg coupling J'_{xy} has precisely the opposite effect: it stabilizes the 1/2 plateau and suppresses the 1/3 one. This competition elucidates the delicate balance between longitudinal and transverse components of the exchange in real RB_4 materials. The conclusion that even weak transverse interactions can significantly reorganize the plateau widths is important because tetraborides are known to exhibit substantial single-ion anisotropy, implying that the experimentally relevant region lies in the regime where J'_{xy} produces an enhancement of the 1/2 plateau consistent with experimental observations.

The mixed-spin formulations and the subsequent mapping to the CDI model represent the final step toward a fully realistic microscopic theory. By incorporating the actual spin magnitudes ($S = 1,\ 3/2,\ 2$) of Tm^{3+}, Er^{3+} and Ho^{3+} ions, the model reproduces the key material-dependent features of the magnetization curves: the stabilization of the 1/2 plateau for $S = 1$ and 3/2 and the persistence of the 1/3 plateau for $S = 2$. This provides a unified explanation for why TmB_4 and ErB_4 behave differently from HoB_4. The CDI mapping allows simulations on significantly larger clusters, confirming the stability of these phases in the thermodynamic limit and offering, for the first time, a realistic

description of both magnetic and thermodynamic responses including the split specific-heat peaks and the magnetocaloric effect.

Finally, the most recent development, the incorporation of charge-stripe potentials, provides a simple yet remarkably effective mechanism for completely suppressing the 1/3 plateau and stabilizing the 1/2 plateau across a wide parameter range. This result is particularly relevant for TmB_4 and ErB_4, where hints of charge modulation have been reported in related borides, and where Jahn–Teller distortions of boron clusters are known to influence the electronic structure. The fact that a periodically modulated local potential can bring the spin–electron model into almost perfect agreement with experiments strongly suggests that charge inhomogeneity is not merely a secondary correction but may represent a missing microscopic ingredient in the full theory of metallic Shastry–Sutherland magnets.

Across all approaches considered in this review, RKKY, spin–electron, Hubbard-enhanced, anisotropic exchange, mixed-spin, CDI, and charge-stripe models, a consistent physical picture emerges. The magnetization processes in rare-earth tetraborides are governed by a robust interplay between itinerant electrons and localized moments, modulated by geometrical frustration and strong single-ion anisotropy. The half-magnetization plateau is an intrinsic and exceptionally stable feature of this interplay, reinforced by electron correlations, transverse spin interactions, and charge modulation. The one-third plateau, while natural in purely localized Ising models, is fragile in metallic systems and survives only when electron correlations, transverse exchange, or charge modulation do not suppress the narrow AF bands that generate it. The overall magnetization sequence and thermodynamic signatures are highly sensitive to the Fermi surface geometry and carrier concentration, explaining the strong material- and doping-dependence observed experimentally.

In conclusion, the combined body of work reviewed here demonstrates that the rare-earth tetraborides form a uniquely rich platform where frustrated magnetism, electronic correlations, anisotropy and itinerancy coexist and interact on equal footing. Theoretical progress over the past decade has transformed our understanding of these materials: from early spin-only models incapable of reproducing experimental curves, to sophisticated correlated spin–electron and CDI frameworks capable of explaining not only the plateau structure, but also specific heat, thermal transitions, magnetocaloric signatures, and charge-spin commensurability. The resulting picture is both conceptually coherent and quantitatively compelling. Yet, important open questions remain, most notably, the microscopic origin and dynamics of possible charge ordering, the role of quantum fluctuations beyond the Ising limit, effects of orbital component, and the degree to which conduction electrons participate in collective excitations in the plateau phases. Addressing these challenges will likely require a combination of advanced numerical techniques, improved experimental resolution, and further refinement of mixed spin–electron models. Nevertheless, the progress to date provides a solid foundation for such future work and firmly establishes the Shastry–Sutherland rare-earth tetraborides as a paradigmatic class of correlated frustrated electron–spin materials.

References

1. B. S. Shastry and B. Sutherland, Exact ground state of a quantum mechanical antiferromagnet, *Physica B+C* 108, 1069 (1981)
2. H. Kageyama, K. Yoshimura, R. Stern, N. V. Mushnikov, K. Onizuka, M. Kato, K. Kosuge, C. P. Slichter, T. Goto, and Y. Ueda, Exact dimer ground state and quantized magnetization plateaus in the two-dimensional spin system $SrCu_2(BO_3)_2$, *Phys. Rev. Lett.* 82(15), 3168 (1999)
3. H. Kageyama, K. Onizuka, T. Yamauchi, Y. Ueda, S. Hane, H. Mitamura, T. Goto, K. Yoshimura, and K. Kosuge, Anomalous magnetizations in single crystalline $SrCu_2(BO_3)_2$, *J. Phys. Soc. Jpn.* 68(6), 1821 (1999)
4. K. Onizuka, H. Kageyama, Y. Narumi, K. Kindo, Y. Ueda, and T. Goto, 1/3 magnetization plateau in $SrCu_2(BO_3)_2$-stripe order of excited triplets, *J. Phys. Soc. Jpn.* 69(4), 1016 (2000)
5. B. Wolf, S. Zherlitsyn, S. Schmidt, H. Schwenk, B. Luthi, H. Kageyama, Y. Ueda, and H. Tanaka, Ultrasonic experiments in $SrCu_2(BO_3)_2$ and NH_4CuCl_3 in magnetic fields up to 50 T, *J. Magn. Magn. Mater.* 226-230, 1973 (2001)
6. K. Kodama, K. Arai, M. Takigawa, H. Kageyama, and Y. Ueda, Spin correlation and field induced staggered magnetization in the 2D orthogonal dimer spin system $SrCu_2(BO_3)_2$, *J. Magn. Magn. Mater.* 272–276, 491 (2004)
7. M. Takigawa, T. Waki, M. Horvatic, and C. Berthier, Novel ordered phases in the orthogonal dimer spin system $SrCu_2(BO_3)_2$, *J. Phys. Soc. Jpn.* 79(1), 011005 (2010)
8. H. Tsujii, C. R. Rotundu, B. Andraka, Y. Takano, H. Kageyama, and Y. Ueda, Specific heat of the $S=1/2$ two-dimensional Shastry–Sutherland antiferromagnet $SrCu_2(BO_3)_2$ in high magnetic fields, *J. Phys. Soc. Jpn.* 80(4), 043707 (2011)
9. D. A. Schneider, K. Coester, F. Mila, and K. P. Schmidt, Pressure dependence of the magnetization plateaus of $SrCu_2(BO_3)_2$, *Phys. Rev. B* 93, 241107(R) (2016)
10. Z. Weihong, C. J. Hamer, and J. Oitmaa, Series expansions for a Heisenberg antiferromagnetic model for $SrCu_2(BO_3)_2$, *Phys. Rev. B* 60(9), 6608 (1999)
11. S. Miyahara and K. Ueda, The magnetization plateaus of $SrCu_2(BO_3)_2$, *Physica B* 281–282, 661 (2000)
12. S. Miyahara and K. Ueda, Theory of the orthogonal dimer Heisenberg spin model for $SrCu_2(BO_3)_2$, *J.*

Phys.: Condens. Matter 15(9), R327 (2003)
13. S. E. Sebastian, N. Harrison, P. Sengupta, C. D. Batista, S. Francoual, E. Palm, T. Murphy, H. A. Dabkowska, and B. D. Gaulin, Fractalization drives crystalline states in a frustrated spin system, *Proc. Natl. Acad. Sci. USA* 105(51), 20157 (2008)
14. P. M. Cônsoli, M. Fornoville, and M. Vojta, Fluctuation-induced ferrimagnetism in sublattice-imbalanced antiferromagnets with application to $SrCu_2(BO_3)_2$ under pressure, *Phys. Rev. B* 104(6), 064422 (2021)
15. T. Verkholyak, J. Strecka, F. Mila, and K. P. Schmidt, Exact ground states of a spin-1/2 Ising–Heisenberg model on the Shastry–Sutherland lattice in a magnetic field, *Phys. Rev. B* 90(13), 134413 (2014)
16. T. Verkholyak and J. Strecka, Fractional magnetization plateaux of a spin-1/2 Heisenberg model on the Shastry –Sutherland lattice: Effect of quantum XY interdimer coupling, *SciPost Phys.* 12, 056 (2022)
17. C. Knetter and G. S. Uhrig, Dynamic structure factor of the two-dimensional Shastry–Sutherland model, *Phys. Rev. Lett.* 92(2), 027204 (2004)
18. V. V. Mazurenko, S. L. Skornyakov, V. I. Anisimov, and F. Mila, First-principles investigation of symmetric and antisymmetric exchange interactions of $SrCu_2(BO_3)_2$, *Phys. Rev. B.* 78(19), 195110 (2008)
19. M. C. Chang and M. F. Yang, Magnetization plateau of the classical Ising model on the Shastry–Sutherland lattice: A tensor renormalization-group approach, *Phys. Rev. B* 79(10), 104411 (2009)
20. P. Corboz and F. Mila, Crystals of bound states in the magnetization plateaus of the Shastry–Sutherland model, *Phys. Rev. Lett.* 112(14), 147203 (2014)
21. P. Czarnik, M. M. Rams, P. Corboz, and J. Dziarmaga, Tensor network study of the $m = 1/2$ magnetization plateau in the Shastry–Sutherland model at finite temperature, *Phys. Rev. B* 103(7), 075113 (2021)
22. K. Kodama, M. Takigawa, M. Horvatic, C. Berthier, H. Kageyama, Y. Ueda, S. Miyahara, F. Becca, and F. Mila, Magnetic superstructure in the two-dimensional quantum antiferromagnet $SrCu_2(BO_3)_2$, *Science* 298(5592), 395 (2002)
23. Z. Shi, S. Dissanayake, P. Corboz, W. Steinhardt, D. Graf, D. M. Silevitch, H. A. Dabkowska, T. F. Rosenbaum, F. Mila, and S. Haravifard, Discovery of quantum phases in the Shastry–Sutherland compound $SrCu_2(BO_3)_2$ under extreme conditions of field and pressure, *Nat. Commun.* 13(1), 2301 (2022)
24. Y. H. Matsuda, N. Abe, S. Takeyama, H. Kageyama, P. Corboz, A. Honecker, S. R. Manmana, G. R. Foltin, K. P. Schmidt, and F. Mila, Magnetization of $SrCu_2(BO_3)_2$ in ultrahigh magnetic fields up to 118 T, *Phys. Rev. Lett.* 111(13), 137204 (2013)
25. M. Takigawa, M. Horvatic, T. Waki, S. Kramer, C. Berthier, F. Levy-Bertrand, I. Sheikin, H. Kageyama, Y. Ueda, and F. Mila, Incomplete Devil's staircase in the magnetization curve of $SrCu_2(BO_3)_2$, *Phys. Rev. Lett.* 110(6), 067210 (2013)
26. A. Liu, J. Zhou, L. Wang, Y. Cao, F. Song, Y. Han, J. Li, W. Tong, Z. Xia, Z. Ouyang, J. Zhao, H. Guo, and Z. Tian, Large magnetocaloric effect in the Shastry–Sutherland lattice compound $Yb_2Be_2GeO_7$ with spin-disordered ground state, *Phys. Rev. B* 110(14), 144445 (2024)
27. A. Liu, F. Song, Y. Cao, H. Ge, H. Bu, J. Zhou, Y. Qin, Q. Zeng, J. Li, L. Ling, W. Tong, J. Sheng, M. Yang, L. Wu, H. Guo, and Z. Tian, Distinct magnetic ground states in Shastry–Sutherland lattice materials: $Pr_2Be_2GeO_7$ versus $Nd_2Be_2GeO_7$, *Phys. Rev. B* 109(18), 184413 (2024)
28. M. Pula, S. Sharma, J. Gautreau, S. K. P, A. Kanigel, M. D. Frontzek, T. N. Dolling, L. Clark, S. Dunsiger, A. Ghara, and G. M. Luke, Candidate for a quantum spin liquid ground state in the Shastry–Sutherland lattice material $Yb_2Be_2GeO_7$, *Phys. Rev. B* 110(1), 014412 (2024)
29. S. Gabáni, K. Flachbart, K. Siemensmeyer, and T. Mori, Magnetism and superconductivity of rare earth borides, *J. Alloys Compd.* 821, 153201 (2020)
30. A. S. Panfilov, G. E. Grechnev, I. P. Zhuravleva, A. V. Fedorchenko, and V. B. Muratov, Specific features of the magnetic properties of RB_4 (R = Ce, Sm and Yb) tetraborides. Effects of pressure, *Low Temp. Phys.* 41(3), 193 (2015)
31. H. Sim, S. Lee, K. P. Hong, J. Jeong, J. R. Zhang, T. Kamiyama, D. T. Adroja, C. A. Murray, S. P. Thompson, F. Iga, S. Ji, D. Khomskii, and J. G. Park, Spontaneous structural distortion of the metallic Shastry–Sutherland system DyB_4 by quadrupole-spin-lattice coupling, *Phys. Rev. B* 94(19), 195128 (2016)
32. J. Fernandez-Rodriguez, J. A. Blanco, P. J. Brown, K. Katsumata, A. Kikkawa, F. Iga, and S. Michimura, Experimental evidence of noncollinear magnetism in gadolinium tetraboride, *Phys. Rev. B* 72(5), 052407 (2005)
33. S. S. Sunku, T. Kong, T. Ito, P. C. Canfield, B. S. Shastry, P. Sengupta, and C. Panagopoulos, Hysteretic magnetoresistance and unconventional anomalous Hall effect in the frustrated magnet TmB_4, *Phys. Rev. B* 93(17), 174408 (2016)
34. H. Yamauchi, N. Metoki, R. Watanuki, K. Suzuki, H. Fukazawa, S. Chi, and J. A. Fernandez-Baca, Magnetic structure and quadrupolar order parameter driven by geometrical frustration effect in NdB_4, *J. Phys. Soc. Jpn.* 86(4), 044705 (2017)
35. N. Metoki, H. Yamauchi, M. Matsuda, J. A. Fernandez-Baca, R. Watanuki, and M. Hagihala, Polarized neutron scattering study of the multiple order parameter system NdB_4, *Phys. Rev. B* 97(17), 174416 (2018)
36. K. Siemensmeyer, E. Wulf, H. J. Mikeska, K. Flachbart, S. Gabani, S. Matas, P. Priputen, A. Efdokimova, and N. Shitsevalova, Fractional magnetization plateaus and magnetic order in the Shastry–Sutherland magnet TmB_4, *Phys. Rev. Lett.* 101(17), 177201 (2008)
37. U. Yu, Ising antiferromagnet on the Archimedean lattices, *Phys. Rev. E* 91(6), 062121 (2015)
38. N. Qureshi, F. Bourdarot, E. Ressouche, W. Knafo, F. Iga, S. Michimura, L. P. Regnault, and F. Duc, Possible stripe phases in the multiple magnetization plateaus in TbB_4 from single-crystal neutron diffraction under pulsed high magnetic fields, *Phys. Rev. B* 106(9),

094427 (2022)
39. J. A. Blanco, P. J. Brown, A. Stunault, K. Katsumata, F. Iga, and S. Michimura, Magnetic structure of GdB_4 from spherical neutron polarimetry, *Phys. Rev. B* 73(21), 212411 (2006)
40. J. Y. Kim, B. K. Cho, and S. H. Han, Anisotropic magnetic phase diagrams of HoB4 single crystal, *J. Appl. Phys.* 105, 07E116 (2009)
41. S. Mataš, K. Siemensmeyer, E. Wheeler, E. Wulf, R. Beyer, Th. Hermannsdorfer, O. Ignatchik, M. Uhlarz, K. Flachbart, S. Gabáni, P. Priputen, A. Efdokimova, and N. Shitsevalova, Magnetism of rare earth tetraborides, *J. Phys. Conf. Ser.* 200(3), 032041 (2010)
42. D. Brunt, G. Balakrishnan, A. R. Wildes, B. Ouladdiaf, N. Qureshi, and O. A. Petrenko, Field-induced magnetic states in holmium tetraboride, *Phys. Rev. B* 95(2), 024410 (2017)
43. D. Brunt, G. Balakrishnan, D. A. Mayoh, M. R. Lees, D. Gorbunov, N. Qureshi, and O. A. Petrenko, Magnetisation process in the rare earth tetraborides, NdB_4 and HoB_4, *Sci. Rep.* 8(1), 232 (2018)
44. S. Yoshii, T. Yamamoto, M. Hagiwara, S. Michimura, A. Shigekawa, F. Iga, T. Takabatake, and K. Kindo, Multistep magnetization plateaus in the Shastry–Sutherland system TbB_4, *Phys. Rev. Lett.* 101(8), 087202 (2008)
45. L. Ye, T. Suzuki, and J. G. Checkelsky, Electronic transport on the Shastry–Sutherland lattice in Ising-type rare-earth tetraborides, *Phys. Rev. B* 95(17), 174405 (2017)
46. S. Michimura, A. Shigekawa, F. Iga, T. Takabatake, and K. Ohoyama, Complex magnetic structures of a Shastry–Sutherland lattice TmB_4 studied by powder neutron diffraction analysis, *J. Phys. Soc. Jpn.* 78(2), 024707 (2009)
47. M. A. Ruderman, and C. Kittel, Indirect exchange coupling of nuclear magnetic moments by conduction electrons, *Phys. Rev.* 96(1), 99 (1954)
48. T. Kasuya, A theory of metallic ferro- and antiferromagnetism on Zener's model, *Prog. Theor. Phys.* 16(1), 45 (1956)
49. K. Yosida, Magnetic properties of Cu–Mn alloys, *Phys. Rev.* 106(5), 893 (1957)
50. J. Trinh, S. Mitra, C. Panagopoulos, T. Kong, P. C. Canfield, and A. P. Ramirez, Degeneracy of the 1 / 8 plateau and antiferromagnetic phases in the Shastry–Sutherland magnet TmB_4, *Phys. Rev. Lett.* 121(16), 167203 (2018)
51. M. Orendáč, S. Gabáni, P. Farkašovský, E. Gažo, J. Kačmarčík, M. Marcin, G. Pristáš, K. Siemensmeyer, N. Shitsevalova, and K. Flachbart, Ground state and stability of the fractional plateau phase in metallic Shastry–Sutherland system TmB_4, *Sci. Rep.* 11(1), 6835 (2021)
52. V. V. Novikov, A. V. Morozov, A. V. Matovnikov, N. V. Mitroshenkov, D. V. Avdashchenko, S. V. Kuznetsov, B. I. Kornev, O. A. Marakhina, V. V. Novikova, and E. O. Bordacheva, The properties of lattice, electronic and magnetic subsystems of erbium tetraboride based on calorimetric data at temperatures of 2–300 K, *J. Alloys Compd.* 581, 431 (2013)
53. R. Watanuki, G. Sato, K. Suzuki, M. Ishihara, T. Yanagisawa, Y. Nemoto, and T. Goto, Geometrical quadrupolar frustration in DyB_4, *J. Phys. Soc. Jpn.* 74(8), 2169 (2005)
54. S. H. Masunaga, V. B. Barbeta, F. Abud, M. S. Torikachvili, and R. F. Jardim, Phase diagram mapping out the complex magnetic structure of single crystals of (Gd, Er)B_4 solid solutions, *Magnetism* 4(1), 24 (2024)
55. S. Mitra, J. G. S. Kang, J. Shin, J. Q. Ng, S. S. Sunku, and T. Kong, P. C. Can eld, B. S. Shastry, P. Sengupta, and Ch. Panagopoulos, Quadratic to linear magnetoresistance tuning in TmB_4, *Phys. Rev. B* 99, 045119 (2019)
56. M. Orendáč, S. Gabáni, E. Gažo, G. Pristáš, N. Shitsevalova, K. Siemensmeyer, and K. Flachbart, Rotating magnetocaloric effect and unusual magnetic features in metallic strongly anisotropic geometrically frustrated TmB_4, *Sci. Rep.* 8, 10933 (2018)
57. M. S. Song, K. K. Cho, J. W. Lee, and B. K. Cho, Abnormal field-dependence of magnetocaloric effect in ErB_4 and TmB_4, *AIP Adv.* 10(2), 025219 (2020)
58. M. S. Song, K. K. Cho, B. Y. Kang, S. B. Lee, and B. K. Cho, Quadrupolar ordering and exotic magnetocaloric effect in RB_4 (R = Dy, Ho), *Sci. Rep.* 10(1), 803 (2020)
59. Z. Y. Meng and S. Wessel, Phases and magnetization process of an anisotropic Shastry–Sutherland model, *Phys. Rev. B* 78(22), 224416 (2008)
60. M. C. Chang and M. F. Yang, Magnetization plateau of the classical Ising model on the Shastry–Sutherland lattice: A tensor renormalization-group approach, *Phys. Rev. B* 79(10), 104411 (2009)
61. Y. Dublenych, Ground states of the Ising model on the Shastry–Sutherland lattice and the origin of the fractional magnetization plateaus in rare-earth-metal tetraborides, *Phys. Rev. Lett.* 109(16), 167202 (2012)
62. Y. Dublenych, Ground states of an Ising model on an extended Shastry–Sutherland lattice and the 1/2-agnetization plateau in some rare-earth-metal tetraborides, *Phys. Rev. E* 88(2), 022111 (2013)
63. Y. Dublenych, Ground-state structures in Ising magnets on the Shastry–Sutherland lattice with long-range interactions and fractional magnetization plateaus in TmB_4, *Phys. Rev. E* 90(5), 052123 (2014)
64. S. A. Deviren, Magnetization plateaus and phase diagrams of the Ising model on the Shastry–Sutherland lattice, *J. Magn. Magn. Mater.* 393, 508 (2015)
65. W. C. Huang, L. Huo, J. J. Feng, Z. B. Yan, X. T. Jia, X. S. Gao, M. H. Qin, and J. M. Liu, Dynamic magnetization process in the frustrated Shastry–Sutherland system TmB_4, *Europhys. Lett.* 102(3), 37005 (2013)
66. H. Čenčariková and P. Farkašovský, Fractional magnetization plateaus in the extended Ising model on the Shastry–Sutherland lattice: Application to rare-earth metal tetraborides, *Phys. Status Solidi B* 252(2), 333 (2015)
67. P. Farkašovský and L. Regeciová, Magnetization plateaus and phase diagrams of the extended Ising model on the Shastry–Sutherland lattice: Effects of long-range interactions, *Eur. Phys. J. B* 92(2), 33

(2019)
68. K. Wierschem, Z. Zhang, A. Wibawa, and P. Sengupta, Magnetization plateaus and supersolid phases in an extended Shastry–Sutherland model, *Eur. Phys. J. B* 91(9), 201 (2018)
69. T. Suzuki, Y. Tomita, and N. Kawashima, Orbital order, stacking defects and spin-fluctuations in the p-electron molecular solid RbO_2, *Phys. Rev. B* 80, 180405(R) (2009)
70. T. Suzuki, Y. Tomita, N. Kawashima, and P. Sengupta, Finite-temperature phase transition to the $m = 1$ 2 plateau phase in the spin-1/2 XXZ model on the Shastry–Sutherland lattices, *Phys. Rev. B* 82(21), 214404 (2012)
71. J. J. Feng, L. Huo, W. C. Huang, Y. Wang, M. H. Qin, J. M. Liu, and Z. Ren, The main 1/2 magnetization plateau in Shastry–Sutherland magnets: Effect of the long-range Ruderman–Kittel–Kasuya–Yosida interaction, *Europhys. Lett.* 105(1), 17009 (2014)
72. L. Regeciová and P. Farkašovský, Influence of the long-range RKKY interaction on a formation of magnetization plateaus in the generalized Ising model on the Shastry–Sutherland lattice, *Acta Phys. Pol. A* 137(5), 625 (2020)
73. L. Regeciová and P. Farkašovský, Magnetic phase diagram of the Ising model with the long-range RKKY interaction, *Eur. Phys. J. B* 92(8), 184 (2019)
74. L. Regeciová and P. Farkašovský, Formation of magnetization plateaus in the 3D Ising model with the long-range RKKY interaction: Application to rare-earth tetraborides, *Eur. Phys. J. B* 93(6), 110 (2020)
75. L. Regeciová and P. Farkašovský, Magnetocaloric effect in the Ising model with RKKY interaction on the Shastry–Sutherland lattice, *Solid State Commun.* 371, 115251 (2023)
76. P. Farkašovský, H. Čenčariková, and S. Mataš, Numerical study of magnetization processes in rare-earth tetraborides, *Phys. Rev. B* 82(5), 54410 (2010)
77. P. Farkašovský and H. Čenčariková, Phase transitions in a coupled electron and spin model on the Shastry–Sutherland lattice, *Acta Phys. Pol. A* 126(1), 44 (2014)
78. P. Farkašovský and L. Regeciová, Formation of magnetization plateaus in rare earth tetraborides: Exact diagonalization and quantum Monte Carlo studies, *J. Supercond. Nov. Magn.* 33(11), 3463 (2020)
79. L. Regeciová and P. Farkašovský, The influence of double-exchange and Heisenberg interaction on magnetization processes in rare-earth tetraborides, *J. Magn. Magn. Mater.* 546, 1687803463 (2022)
80. P. Farkašovský and L. Regeciová, Ground states and thermodynamics of the spin–electron model with mixed spins: Application to rare-earth tetraborides, *Physica E* 143, 115396 (2022)
81. P. Farkašovský and L. Regeciová, Ground state and thermodynamic properties of the coupled double-Ising model: application to rare-earth tetraborides, *J. Phys.: Condens. Matter* 34(43), 435802 (2022)
82. L. Regeciová and P. Farkašovský, Magnetization processes and magnetocaloric effect in the two-dimensional coupled double-Ising model, *Physica B* 650, 414514 (2023)
83. P. Farkašovský, Impact of charge stripes on magnetization processes in rare-earth tetraborides, *J. Magn. Magn. Mater.* 629, 173284 (2025)
84. M. E. J. Newman and G. T. Barkema, Monte Carlo Methods in Statistical Physics, Oxford University Press, New York, 2010
85. D. J. Earlab and M. W. Deem, Parallel tempering: Theory, applications, and new perspectives, *Phys. Chem. Chem. Phys.* 7, 3910 (2005)
86. M. T. Beal-Monod, Ruderman–Kittel–Kasuya–Yosida indirect interaction in two dimensions, *Phys. Rev. B* 36, 8835 (1987)
87. R. Lemański, Model of charge and magnetic order formation in itinerant electron systems, *Phys. Rev. B* 71(3), 035107 (2005)
88. R. Lemański and J. Wrzodak, Ground-state phase diagrams of the generalized Falicov–Kimball model with Hund coupling, *Phys. Rev. B* 78(8), 085118 (2008)
89. P. Farkašovský and H. Čenčariková, Ground states of the generalized Falicov–Kimball model in one and two dimensions, *Eur. Phys. J. B* 47(4), 517 (2005)
90. P. Farkašovský, Enhancement of the d -wave pairing correlations by charge and spin ordering in the spin-one-half Falicov–Kimball model with Hund and Hubbard coupling, *Europhys. Lett.* 115(3), 37006 (2016)
91. P. Farkašovský, Influence of spin ordering on superconducting correlations in the spin-one-half Falicov–Kimball model with Hund and Hubbard coupling, *J. Supercond. Nov. Magn.* 30(3), 581 (2017)
92. P. Farkašovský, Ground-state properties of the Falicov –Kimball model in one and two dimensions, *Eur. Phys. J. B* 20(2), 209 (2001)
93. M. S. Challa, D. P. Landau, and K. Binder, Finite-size effects at temperature-driven first-order transitions, *Phys. Rev. B* 34(3), 1841 (1986)
94. E. Dagotto, Correlated electrons in high-temperature superconductors, *Rev. Mod. Phys.* 66(3), 763 (1994)
95. D. D. Betts, S. Masui, N. Vats, and G. E. Stewart, Improved finite-lattice method for estimating the zero-temperature properties of two-dimensional lattice models, *Can. J. Phys.* 74(1-2), 54 (1996)
96. D. D. Betts, H. Q. Lin, and J. S. Flynn, Improved finite-lattice estimates of the properties of two quantum spin models on the infinite square lattice, *Can. J. Phys.* 77(5), 353 (1999)
97. S. Sorella, S. Baroni, R. Car, and M. Parrinello, A novel technique for the simulation of interacting fermion systems, *Europhys. Lett.* 8(7), 663 (1989)
98. E. Y. Loh and J. E. Gubernatis, in: Modern Problems of Condensed Matter Physics, edited by W. Hanke and Y. Kopaev, North Holland, Amsterdam, 1992
99. M. Imada and Y. Hatsugai, Numerical studies on the Hubbard model and the t–J model in one- and two-dimensions, *J. Phys. Soc. Jpn.* 58(10), 3752 (1989)
100. M. Cyrot, The Hubbard hamiltonian, *Physica B+C* 91, 141 (1977)
101. A. Azarevich, V. Glushkov, S. Demishev, A. Bogach, V. Voronov, S. Gavrilkin, N. Shitsevalova, V. Filipov,

S. Gabáni, J. Kačmarčík, K. Flachbart, and N. Sluchanko, Evidence of symmetry lowering in antiferromagnetic metal TmB_{12} with dynamic charge stripes, *J. Phys.: Condens. Matter* 34(6), 065602 (2022)

102. N. B. Bolotina, O. N. Khrykina, A. N. Azarevich, N. Y. Shitsevalova, V. B. Filipov, S. Y. Gavrilkin, K. V. Mitsen, V. V. Voronov, and N. E. Sluchanko, Checkerboard patterns of charge stripes in the two-gap superconductor ZrB_{12}, *Phys. Rev. B* 105(5), 054511 (2022)
103. A. P. Dudka, O. N. Khrykina, N. B. Bolotina, N. Y. Shitsevalova, V. B. Filipov, M. A. Anisimov, S. Gabani, K. Flachbart, and N. E. Sluchanko, Quantum diffusion regime of charge transport in GdB_6 caused by electron and lattice instability, *Phys. Rev. B* 100(20), 205103 (2019)
104. N. E. Sluchanko, A. N. Azarevich, A. V. Bogach, N. B. Bolotina, V. V. Glushkov, S. V. Demishev, A. P. Dudka, O. N. Khrykina, V. B. Filipov, N. Y. Shitsevalova, G. A. Komandin, A. V. Muratov, Y. A. Aleshchenko, E. S. Zhukova, and B. P. Gorshunov, Observation of dynamic charge stripes in $Tm_{0.19}Yb_{0.81}B_{12}$ at the metal–insulator transition, *J. Phys.: Condens. Matter* 31(6), 065604 (2019)
105. O. N. Khrykina, N. B. Bolotina, V. M. Gridchina, A. N. Azarevich, A. V. Bogach, S. V. Demishev, K. M. Krasikov, N. Y. Shitsevalova, V. B. Filipov, and N. E. Sluchanko, Evidence for nanosized magnetic clusters of Ce-ions in the archetypal heavy fermion metal CeB_6, *J. Alloys Comp.* 970. 172527 (2024)
106. N. B. Bolotina, A. P. Dudka, O. N. Khrykina, V. N. Krasnorussky, N. Y. Shitsevalova, V. B. Filipov, and N. E. Sluchanko, The lower symmetry electron-density distribution and the charge transport anisotropy in cubic dodecaboride LuB_{12}, *J. Phys:. Condens. Matter* 30(26), 265402 (2018)
107. T. A. Maier, G. Alvarez, M. Summers, and T. C. Schulthess, Dynamic cluster quantum Monte Carlo simulations of a two-dimensional Hubbard model with stripe-like charge-density-wave modulations: Interplay between inhomogeneities and the superconducting state, *Phys. Rev. Lett.* 104(24), 247001 (2010)
108. R. Mondaini, T. Ying, T. Paiva, and R. T. Scalettar, Determinant quantum Monte Carlo study of the enhancement of *d*-wave pairing by charge inhomogeneity, *Phys. Rev. B* 86(18), 184506 (2012)
109. Ch. Chen, P. Zhong, X. Sui, R. Ma, Y. Liang, S. Hu, T. Ma, H. Q. Lin, and B. Huang, Author correction: Charge stripe manipulation of superconducting pairing symmetry transition, *Nat. Commun.* 15(1), 10647 (2024)